

Research papers

Numerical investigations of steam accumulator dynamics: Assessment of computational models



Milica Ilic ^{a,*}, Vladimir D. Stevanovic ^b, Milan M. Petrovic ^b, Sanja Milivojevic ^b

^a University of Belgrade, Innovation Center of the Faculty of Mechanical Engineering, Kraljice Marije 16, 11120 Belgrade, Serbia

^b University of Belgrade, Faculty of Mechanical Engineering, Kraljice Marije 16, 11120 Belgrade, Serbia

ARTICLE INFO

Keywords:

Thermal energy storage
Steam accumulators
Numerical modelling
Liquid-steam two-phase system
Evaporation/condensation

ABSTRACT

Steam accumulators are crucial components of systems for thermal energy storage in various facilities utilizing either fossil or renewable energy source. Accurate predictions of steam accumulator dynamics are of immense importance for the proper design and the reliable operation of these storage systems. For this purpose, the numerical modelling of transient behaviour of two-phase steam-liquid water system within the steam accumulator is applied in the majority of reported investigations. It is observed that there are differences in these applied modelling approaches, which raises concerns regarding their validity. In that regard, this paper deals with assessment of contemporary computational models for numerical investigations of the steam accumulator dynamics. The focus is placed on modelling approaches based on differential mass and energy balance equations of the two-phase steam-liquid water system in the steam accumulator. Models based on assumption of either thermal equilibrium or thermal non-equilibrium between phases are considered. The validity of both, the structure of governing equations and the applied closure laws are investigated using available measured data.

The results of conducted analyses show that in some modelling approaches the energy equation is not correctly formulated. Therefore, some terms in this equation associated with the transfer processes at the steam-liquid water interface are either omitted or abundant, which leads to erroneous numerical results. Further, the heat transfer to the walls of the steam accumulator vessel may not be neglected as it affects dynamics of the two-phase system not only during, but also after the transient. Finally, the heat transfer due to the difference in temperature between liquid water and steam needs to be accounted for. Otherwise, the steam temperature could attain unphysically high values.

The critical issue in closure laws for the evaluation of mass transfer rate at the phase interface is the so-called relaxation factor, which accounts for a finite time of the phase transition. Commonly, this parameter is either adopted as empirical constant or estimated by experimental investigations of the considered steam accumulator. The existing methodology for the theoretical determination of the relaxation factor turned out to be of limited applicability. This paper introduces an improved relation for evaluation of the relaxation factor, which takes into account the geometry of the steam accumulator, i.e. the dependance of the interfacial area concentration for the phase transition on the ratio of the wetted walls area to the liquid volume. The relation is validated using available data measured during the charging of industrial and lab-type steam accumulators.

1. Introduction

Steam accumulators are devices used to store thermal energy in wide range of industries (chemical, food, textile, etc.) and power plants (solar, nuclear, fossil-/biomass-fueled). In these facilities, the steam accumulators serve as buffers between steam generators and steam consumers and dampen imbalances between variable steam production and

demand. The peculiarity of steam accumulators is the use of water as both the heat transfer medium (steam) and the storage medium (liquid water) [1].

As described by Steinmann [1] there are three basic types of steam accumulators: (a) the sliding pressure (also called Ruths storage) steam accumulators, (b) the expansion steam accumulators and (c) the displacement steam accumulators. In the two latter cases, steam is

* Corresponding author.

E-mail addresses: milic@mas.bg.ac.rs (M. Ilic), vstevanovic@mas.bg.ac.rs (V.D. Stevanovic), mlpetrovic@mas.bg.ac.rs (M.M. Petrovic), smilivojevic@mas.bg.ac.rs (S. Milivojevic).

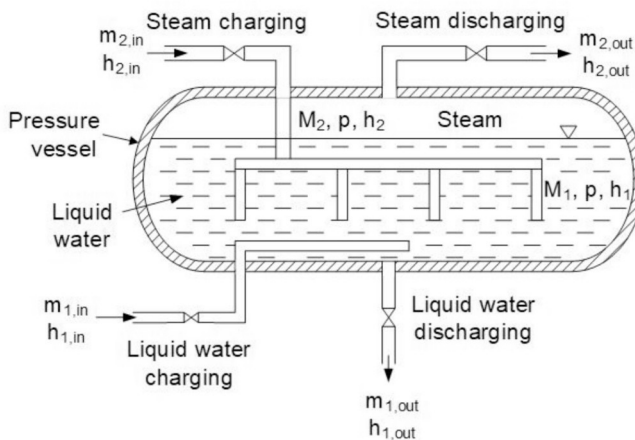


Fig. 1. Layout of steam accumulator with charging/discharging attachments.

generated by flashing of hot water from the accumulator pressure vessel, which is discharged into an external expansion vessel. The pressure vessel in case of the expansion steam accumulator is filled with hot water and the small steam cushion on the top. Hot water is discharged at the bottom of the pressure vessel. The displacement steam accumulator is based on thermocline effect – the upper part of the pressure vessel is occupied by hot water, while its lower part is filled with cold water. Hot water is discharged from the top of the pressure vessel. Different to the expansion and displacement steam accumulator types, in the case of the steam accumulator of Ruths storage type, steam is generated internally by flashing of hot water within the pressure vessel.

In this paper, under the term “steam accumulator” the Ruths storage is meant. The layout of this type of steam accumulator is schematically presented in Fig. 1 and its operation is described in the following.

During the energy storage process (commonly called the charging of steam accumulator) the steam with the mass flow rate $m_{2,in}$ and the enthalpy $h_{2,in}$ is injected into the liquid water through the system of perforated tubes. The heat transferred due to the steam condensation increases the enthalpy h_1 and the energy density of the liquid water storing in that way the heat. Accordingly, the mass of liquid water M_1 in the steam accumulator needs to be large (the volumetric content of liquid water in the steam accumulator can be as high as 90 % of the steam accumulator volume V) in order to provide the amount of stored energy as high as possible. When the stored energy is released (process commonly called the discharging of steam accumulator), the steam with the mass flow rate $m_{2,out}$ and the enthalpy $h_{2,out}$ is let out from the steam accumulator. Due to discharging, the pressure in the steam accumulator p decreases causing flashing and generation of steam of the enthalpy h_2 . In that way, the energy stored in the liquid water is retrieved. The liquid water inflow $m_{1,in}h_{1,in}$ is open only when the level of the liquid phase is below the desired value, while the liquid water outlet is used only for drainage of the steam accumulator during maintenance. In that regard, the charging/discharging of steam accumulator is related to the inflow/outflow of steam.

The transient processes of the steam accumulator charging/discharging are associated with complex mechanisms such as: (i) the direct contact condensation of steam jets injected into the liquid water pool, (ii) the steam generation during adiabatic evaporation of superheated water and its separation to the steam space of steam accumulator, (iii) the heat transfer at phase interface due to different temperatures of steam and liquid water and (iv) the heat transfer between steam/liquid water and walls of the steam accumulator pressure vessel.

The complexity of the above-mentioned physical mechanisms as well as their mutual interplay make the mathematical formulation of steam accumulator dynamics an extremely difficult task. Consequently, the models of transient behaviour of steam accumulators are developed

introducing several assumptions. First, the steam-liquid system within the steam accumulator is described by the so-called lumped parameter model in which spatial changes are neglected and only the temporal evolution of system variables is considered. Next, the mechanical equilibrium is assumed, i.e. the unique pressure for both the liquid water and the steam. Regarding the thermal state of phases, there are two approaches. The *equilibrium* models are based on the assumption that the temperature of both the steam and the liquid water are determined by the governing pressure p , i.e. equal to the saturation temperature $T_{sat}(p)$. Therefore, when applying this model, it is sufficient to determine the evolution of pressure and vapour content during the course of transient to be able to derive all other relevant quantities. On the other side, the *non-equilibrium* models take into account the thermal non-equilibrium between liquid and steam, which necessitates posing balance equations of mass and energy for each phase. Further, in order to complete the non-equilibrium models, closure laws for mass and energy rates due to the phase transition and the heat transfer between phases are necessary. The literature survey shows that either *equilibrium* or *non-equilibrium* models are applied to numerically investigate the dynamics of steam accumulators in various configurations. The most relevant examples of steam accumulator modelling are presented in the text below.

Stevanovic et al. [2] developed the *non-equilibrium* model for the investigation of steam accumulator dynamics within a coal drying plant (accumulator volume $V = 64 \text{ m}^3$, design pressure $p = 50 \text{ bar}$). The closure laws for the condensation (m_c) and evaporation (m_e) rate are formulated by introducing an empirical parameter named relaxation factor (τ_k , $k = c$ for condensation, $k = e$ for evaporation) which takes into account that the phase transition is not instantaneous, but occurs within finite time. The comparison of data measured during steam accumulator charging with corresponding numerical results has shown that good agreement is obtained when $\tau_c = 85 \text{ s}$. The heat transfer rate due to temperature difference between phases is formulated adopting the constant value of the product of heat transfer coefficient and interfacial area concentration $(ha)_{21} = 50 \cdot 10^3 \text{ W/m}^3\text{K}$. In their later paper Stevanovic et al. [3] developed a method for the evaluation of τ_k ($k = c, e$) and $(ha)_{21}$ considering the mass flux at the phase interface and the interfacial area concentration as key variables. The former is formulated by applying an empirical relation for the heat transfer coefficient between the liquid water and the bubble surface, while the latter relies on empirical correlations for the bubble diameter and the bubble concentration in the flashing nozzle flows. The method is validated for the case of the above-mentioned steam accumulator within coal drying plant. Stevanovic et al. [3] also present derivation of the *equilibrium* model of steam accumulator. Both models of Stevanovic et al. [3], the equilibrium one and the non-equilibrium one, have been used in number of publications for numerical investigations of steam accumulator dynamics in various facilities.

Another comprehensive paper is published by Sun et al. 2015 [4], who presented examinations of a lab-type steam accumulator (volume $V = 1.12 \text{ m}^3$). The presented research involves numerical computations accounting for *non-equilibrium* effects and corresponding experimental investigations. The experimental campaign encompasses three sets of charging and two sets of discharging cases. In the charging cases, the following quantities were varied: the pressure (6.63–13.9 bar), the temperature (280.2–293 °C) and the mass flow rate (0.2–0.21 kg/s) of the inlet superheated steam as well as the initial pressure in the steam accumulator (4.84–8.62 bar). The discharging experiments have been conducted for two values of the initial pressure: 11.5 bar and 5.9 bar. The comparison of measured data and numerical results has shown that the relaxation factor takes values $\tau_c = 8\text{--}9.5 \text{ s}$ for the charging cases and $\tau_e = 1\text{--}1.4 \text{ s}$ for the discharging ones.

Raphael et al. [5] applied the *non-equilibrium* model to investigate the application of steam accumulator as a buffer storage in a desalination plant coupled with the linear Fresnel reflector solar unit. The transient behaviour of steam accumulator of volume $V = 12 \text{ m}^3$ is

simulated during charging and discharging, which depends on the vapour generation in the solar plant within the period 9–23 h of normal as well as of disturbed solar irradiance. In addition, computations have been performed using the volume of steam accumulator as parameter (V varied in the range of 4–16 m³).

Non-equilibrium effects were also accounted for by Richter et al. [6] and by Stevanovic et al. [7], who dealt with implementation of steam accumulators into coal-fired thermal power plants with the goal to increase plant flexibility. Richter et al. [6] envisaged the charging of steam accumulator with the cold reheat steam (pressure 40 bar and temperature 310 °C) and its discharging to the high-pressure feed water heaters (pressure 20 bar). This configuration requires the volume for steam accumulation $V = 1331$ m³ to provide 30 min long discharging time within a 730 MWe power plant. Stevanovic et al. [7] studied the installation of steam accumulator of 600 m³ in a 650 MWe power plant. In their solution, the steam accumulator is also charged by the cold reheat steam (pressure 45 bar and temperature 334.9 °C). However, the discharging is foreseen into two condensate heaters (pressure 2.3 bar and 5.6 bar).

The modelling of steam accumulator dynamics was also performed for various hybrid storage systems. Yu et al. [8] considered the hybrid storage system installed in a 1 MWe solar power plant. The system consists of the steam accumulator ($V = 100$ m³, $p = 24$ bar) and two oil tanks (before charging of the accumulator the superheated steam from the central receiver is cooled in the cold oil tank; the steam discharged from the steam accumulator is superheated in the hot oil tank and then led to the turbine). The dynamics of the steam accumulator is computed applying the *non-equilibrium* model which is significantly different from the one presented by Stevanovic et al. [2,3]. This model by Yu et al. [8] strongly relates to the one presented by Xu et al. [9] which is used for similar purpose – the modelling of steam accumulator within a thermal energy storage system in the 1 MWe solar power plant.

Another type of hybrid storage system involves concrete blocks in which the saturated steam from the steam accumulator is superheated. Stark et al. [10] applied the *equilibrium* model to numerically investigate the steam accumulator dynamics within a biomass-fueled combined heat and power plant. In this solution, the superheated fresh steam extracted from the boiler passes through the concrete blocks and then charges the steam accumulator. In the reverse direction, the saturated steam discharged from the steam accumulator is superheated in the concrete blocks before it enters the auxiliary turbine. The parametric analysis was conducted by varying the volume of the steam accumulator ($V = 50$ –300 m³) for the charging process and the mass flow rate of the outlet steam ($m_{2,out} = 2.5$ –5.5 kg/s) for the discharging process. Gonzalez-Gomez et al. [11] considered the implementation of the hybrid steam accumulation system with concrete blocks in a combined power plant (gas turbine and steam cycle) with the goal to recover a portion of steam energy during plant start-ups. The system involves 8 steam accumulators (volume of each 197 m³, design pressure 25 bar). Before entering the steam accumulators, steam passes through 1310 tubes within cylindrical concrete blocks. The saturated steam discharged from the steam accumulator is superheated in the concrete blocks reaching the required parameters for supply of the intermediate pressure turbine. The simulation of steam accumulator dynamics was done by the *equilibrium* model. Kindi et al. [12] also studied the hybrid system with the concrete blocks for an improvement of the steam accumulation system in the 50 MWe Khi Solar One power plant. The original storage system of this plant consists of two groups of steam accumulators: 16 base steam accumulators (volume of each 197 m³) and 3 superheating accumulators (volume of each 197 m³) at higher pressure and temperature. Steam from the superheating accumulators is used to superheat the steam from the base steam accumulators in the storage superheater before its entrance to the turbine. In the advanced option, all 19 units would be used as the base steam accumulators, while the concrete blocks would be applied to store the energy of charging steam from the power plant superheater. The *equilibrium* model is applied to perform numerical

analysis of the steam accumulator dynamics. The computations were performed for the case of the diurnal operation of Khi Solar One plant, which involves both the charging and discharging of the system for thermal energy storage.

Dynamics of steam accumulation is also considered in the hybrid storage systems which consist of the steam accumulator and phase-change material (PCM). In such systems, the PCM serves as the latent heat thermal energy storage which absorbs/releases heat. Dusek and Hofmann [13] applied the *equilibrium* model to study a storage system in which the steam accumulator (cylindrical vessel with inner diameter 2.7 m and length 9.6 m) is wrapped with 6 concentrically positioned 5 cm thick PCM modules. The applied model was validated by measured data obtained on the steam accumulator system in the Austrian steel manufacturer Voestalpine Stahl Donawitz GmbH. The system consists of three interconnected steam accumulators: the smaller one with the geometry presented above and two larger ones with the inner diameter 3.1 m and length 10.7 m. The computations were performed for two cases where the accumulators are charged by one or two steam generators. Kasper et al. [14] developed and experimentally tested a lab-scale prototype of the PCM hybrid storage system proposed by Dusek and Hofmann [13]. The prototype steam accumulator is scaled down to the inner diameter 0.686 m and the cylindrical length 2.319 m. The 8 PCM modules with 3 cm thick PCM layer are distributed along the steam accumulator perimeter covering the angle of 133.5°. The dynamics of the steam accumulator is numerically investigated by applying the *equilibrium* model. The model is validated by corresponding data (pressure, temperature, liquid level) measured during a complex transient which involves charging as well as discharging. Niknam and Sciacovelli [15] considered the application of hybrid PCM steam accumulator system within a food processing factory. The steam accumulator (diameter 2 m and length 8.4 m) was charged by saturated steam at 26 bar. The discharging starts at 20 bar. The thickness of PCM layer was used as model parameter (2 cm, 4 cm and 7 cm). The dynamics of steam - liquid mixture within the steam accumulator was computed using the *non-equilibrium* model.

As shown in the text above, steam accumulators play an important role as components of thermal energy storage systems in numerous facilities. In these facilities, various steam accumulators are applied regarding their size, working pressure, charging steam parameters and other operating conditions. Taking this into account, it is questionable, whether all various states can be properly described by the steam accumulator models. Here is an example. The above-presented data of Stevanovic et al. [3] and Sun et al. [4] show that value of relaxation factor τ_c significantly changes with change of accumulator volume. Moreover, for the same accumulator, the relaxation factors τ_c and τ_e differ significantly.

As in majority of publications the design and operation of corresponding thermal energy systems as well as their reliable coupling with components of the main facility are based on the modelling of steam accumulator dynamics during transients caused by accumulator charging/discharging, the above issue needs to be examined carefully. In that regard, this paper deals with the accuracy of models applied to formulate mechanisms taking place in the steam - liquid water two-phase system of the steam accumulator.

The contribution of the paper is twofold. First, comprehensive analysis of contemporary applied numerical models for computation of the steam accumulator dynamics is given. Second, the paper gives a detailed assessment of these models through the comparison of computational results with available experimental data and on this basis proposes their possible improvement. In this framework, the applicability of the *equilibrium* model is estimated. Next, the *non-equilibrium* model is thoroughly surveyed. The structure of governing equations in different forms of this model is studied based on the theoretical case of an open thermodynamic system and according to the model performance. A special attention is paid on the analysis of applied closure laws, particularly on the relaxation factor τ_k ($k = c, e$) as it affects the values of

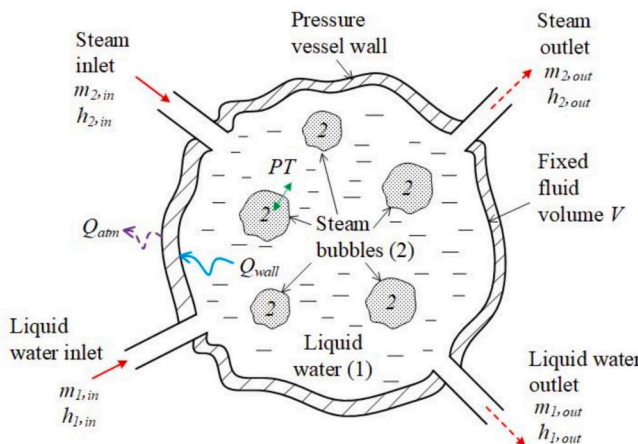


Fig. 2. Schematic presentation of lumped parameter model of the steam accumulator.

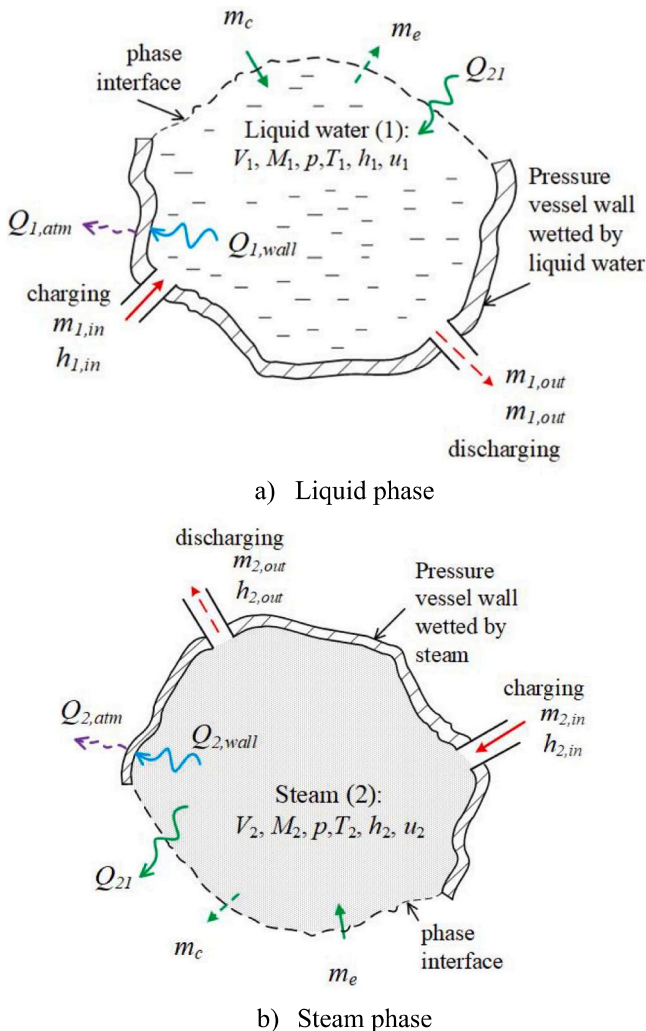


Fig. 3. Physical model of steam accumulator in non-equilibrium modelling approach with separated liquid and steam phase.

extremely important condensation (m_c) and evaporation (m_e) terms. Finally, the paper presents improved methodology for the formulation of relaxation factor, which is validated by available measured data obtained for charging of steam accumulators of different size.

2. Analysis of contemporary approaches for modelling of steam accumulator dynamics

The contemporary approaches for the modelling of steam accumulator dynamics are based on the lumped parameter model for two-phase gas-liquid mixture as schematically presented in Fig. 2. The steam accumulator is considered as an open thermodynamic system with fixed volume V and attachments for inflow and outflow of liquid water (denoted with subscript 1) and steam (denoted with subscript 2). In Fig. 2 the mass flow rate and specific enthalpy of the fluid at the attachments are denoted by m and h , while the subscripts in and out represent inlet and outlet.

Some heat from the two-phase system is transferred to the walls of pressure vessel as schematically presented in Fig. 2 (denoted by Q_{wall}). We note that the largest part of Q_{wall} is accumulated in the vessel walls and a slight portion is dissipated to the surrounding atmosphere through thermal insulation (denoted by Q_{atm} in Fig. 2). Depending on a transient, the two-phase mixture in the steam accumulator can undergo either pressurization or depressurization, which causes interface phase transfer (denoted by PT in Fig. 2) of mass and heat as well as the change of liquid water/steam thermal state.

In the lumped parameter model of the steam accumulator, the specific enthalpy h and the pressure p of the steam - liquid water mixture are averaged spatially. The mixture is in mechanical equilibrium i.e. both phases are stagnant and at the same pressure p . Under these conditions, the system can be described by the balance equations for mass and energy. The energy balance equation for the two-phase mixture within the steam accumulator is derived by adjusting the energy conservation law for an open thermodynamic system (for consistency reasons this law is given in Appendix 1). Depending on how the thermal state of phases is considered, one can distinguish between the non-equilibrium and equilibrium models as presented in Sections 2.1 and 2.2, respectively.

2.1. Non-equilibrium models of steam accumulator dynamics

In the *non-equilibrium* modelling approach, the phases are considered separately. Each phase represents an open thermodynamic system with its own quantities as presented in Fig. 3. The dynamics of liquid water (phase 1) and steam (phase 2) is formulated by balance equations presented in Section 2.1.1. The exchange between phases in the form of mass transfer (condensation m_c or evaporation m_e) and heat transfer due to the temperature difference between phases (Q_{21}) is described by closure laws as presented in Section 2.1.2.

2.1.1. Governing equations of non-equilibrium models

Tables 1–4 present four variants of governing equations implemented in non-equilibrium models of the steam accumulator. First, the applied energy conservation equation is compared with Eq. (A8) or Eq. (A7) from Appendix 1. Next, a derivation of differential equation for pressure change is presented, when possible. In that framework, balance equations for mass of phase i ($i = 1, 2$) are given. Finally, the correctness of presented equations is commented.

2.1.2. Closure laws in non-equilibrium models

In each non-equilibrium model, the set of governing differential equations is completed with closure laws. In this Section, closure laws applied in non-equilibrium models I–III are outlined. We remind that for the non-equilibrium model IV no closure laws are presented in the corresponding publication.

2.1.2.1. Evaporation and condensation rate. In the non-equilibrium model I both evaporation and condensation rate (m_e and m_c) are related to the thermal state of the liquid water. Accordingly, the specific enthalpy h_1 is compared to the specific enthalpy of saturated liquid water h' . The evaporation occurs when the liquid water is superheated:

Table 1

Non-equilibrium model I - governing equations.

Terms in energy balance equation presented in form of Eq. (A8)					Eq.	Applied in:
L ₁	R ₁	R ₂	R ₃	R ₄		
$\frac{d(Mh)_i}{dt} = Q_{i,TD} + (mh)_{i,PT} + V_i \frac{dp}{dt} + m_{i,in}h_{i,in} - m_{i,out}h_i$					(1)	[2–5,7,15]

Analysis:

The comparison with Eq. (A8) shows that in energy balance Eq. (1) all terms are included. The outlet enthalpy is adopted to be equal to the phase enthalpy $h_{i,out} = h_i$ as presented by the term R₄. The term R₁ consists of two parts. The first part accounts for the heat transfer rate due to the difference in temperatures of steam and liquid water $\Delta T_{21} = T_2 - T_1$. When $\Delta T_{21} > 0$, $Q_{i,TD} = (-1)^{i+1}Q_{21}$, while in opposite case $Q_{i,TD} = (-1)^iQ_{21}$, where Q_{21} stands for the heat transfer rate between phases as presented in Section 2.1.2.2. The second part of R₁ term represents the heat transfer rate due to the phase transition $(mh)_{i,PT} = (-1)^{i+1}(m_c - m_e)h'$, where h' denotes the enthalpy of saturated steam and the mass flow rates due to condensation m_c and evaporation m_e are formulated in Section 2.1.2.1. The heat transfer rate $Q_{i,wall}$ between the walls of steam accumulator vessel and phase i ($i = 1, 2$) is neglected. Derivation of differential equation for dp/dt . The starting point for derivation of dp/dt equation is the volume balance equation of steam accumulator:

$$V = \sum_{i=1,2} V_i = \sum_{i=1,2} M_i v_i. \quad (2)$$

Eq. (2) can be rearranged to:

$$\sum_{i=1,2} v_i \frac{dM_i}{dt} + \sum_{i=1,2} M_i \left(\frac{\partial v_i}{\partial p} \frac{dp}{dt} + \frac{\partial v_i}{\partial h} \frac{dh}{dt} \right) = 0. \quad (3)$$

as specific volume is $v_i = v_i(p, h_i)$. The mass conservation of phase i is given by:

$$\frac{dM_i}{dt} = m_{i,in} - m_{i,out} + (-1)^{i+1}(m_c - m_e). \quad (4)$$

The time derivative of specific enthalpy h_i can be evaluated from Eq. (1) as:

$$\frac{dh_i}{dt} = \frac{1}{M_i} \left[(mh)_{i,in} - (mh)_{i,out} + (-1)^{i+1}(m_c - m_e)h' + Q_{i,TD} + M_i v_i \frac{dp}{dt} - h_i \frac{dM_i}{dt} \right]. \quad (5)$$

Substituting Eqs. (4) and (5) into Eq. (3) gives the pressure change with time t :

$$\frac{dp}{dt} = \frac{\sum_{i=1,2} \left(h_i \frac{\partial v_i}{\partial h} - v_i \right) \frac{dM_i}{dt} - \sum_{i=1,2} \left[(mh)_{i,in} - (mh)_{i,out} + (-1)^{i+1}(m_c - m_e)h' + Q_{i,TD} \right] \frac{\partial v_i}{\partial h}}{\sum_{i=1,2} \left(\frac{\partial v_i}{\partial p} + v_i \frac{\partial v_i}{\partial h} \right) M_i}. \quad (6)$$

$$m_e = \frac{M_1(h_1 - h')}{\tau_e r} \quad \text{for } h_1 > h', \quad (14)$$

while the steam condenses when the liquid water is subcooled:

$$m_c = \frac{M_1(h' - h_1)}{\tau_c r} \quad \text{for } h_1 < h', \quad (15)$$

otherwise, m_e and m_c are zero valued. In the above relations τ_e and τ_c respectively represent the relaxation factor (also named relaxation time) for evaporation and condensation.

In majority of reported investigations, empirical values of τ_e and τ_c are used. These values are estimated by use of experimental data - the values of τ_e and τ_c are adjusted until the computed and measured data for pressure during the steam accumulator transient reach satisfactory agreement. Table 5 presents values of τ_e and τ_c determined in this way for different types of steam accumulators and different operating conditions.

The evaluation of τ_e and τ_c based on theoretical considerations was reported by Stevanovic et al. [3]. For consistency, this approach is presented here briefly. The interfacial mass transfer rate per unit of liquid volume Γ_k is expressed as product of the interfacial area concentration a_{21} and the interfacial mass flux j_k :

$$\Gamma_k = m_k / V_1 = a_{21} j_k, \quad (16)$$

where the subscript k denotes phase transition ($k = e$ evaporation, $k = c$ condensation). Substituting Eq. (14) as well Eq. (15) in the above expression gives the following relation:

$$\Gamma_k = \frac{\rho_1 |h_1 - h'|}{\tau_k r} = a_{21} j_k, \quad (17)$$

what enables the formulation of the relaxation factor:

$$\tau_k = \frac{\rho_1 |h_1 - h'|}{j_k a_{21} r}. \quad (18)$$

The phase transition mass flux j_k ($k = e, c$) in the above relation is evaluated from:

$$j_k = \frac{k_{1,int} |T_1 - T_{sat}|}{r}, \quad (19)$$

where $k_{1,int}$ stands for the heat transfer coefficient between steam bubble phase interface and surrounding liquid water [16]:

$$k_{1,int} = \frac{\lambda_1}{D_b} (2 + 0.74 Re_b^{1/2} Pr_1^{1/3}). \quad (20)$$

The thermal conductivity and Prandtl number of liquid water are respectively denoted by λ_1 and Pr_1 , while bubble Reynolds number is computed as:

Table 2

Non-equilibrium model II - governing equations.

Terms in energy balance equation presented in form of Eq. (A8)				
L ₁	R ₁	R ₂	R ₃	R ₄
$\frac{d(Mh)_i}{dt} = (mh)_{i,PT} + 0 + m_{i,in}h_{i,in} - m_{i,out}h_i$				(7) [8]

Analysis:

The comparison with Eq. (A8) shows that the term R₃ ($V_i dp/dt$) is omitted from Eq. (7). Therefore, the energy balance Eq. (7) is incomplete. The term R₂ accounts only for $(mh)_{i,PT}$ while $Q_{i,TD}$ and $Q_{i,wall}$ ($i = 1,2$) are neglected. The heat transfer rate due to the phase transition is formulated as $(mh)_{i,PT} = (-1)^{i+1}(m_e h_2 - m_e h')$. The comparison with the non-equilibrium model I shows that h_2 is used instead of h' as the enthalpy relevant for the heat transfer rate due to condensation.

Derivation of differential equation for dp/dt . The starting point for derivation of dp/dt equation is the decomposition of time derivative of steam mass:

$$\frac{dM_2}{dt} = \frac{d}{dt}(\rho_2 V_2) = V_2 \frac{d\rho_2}{dt}. \quad (8)$$

As steam density is $\rho_2 = \rho_2(p, h_2)$, the above equation can be rearranged to:

$$\frac{dM_2}{dt} = V_2 \frac{\partial \rho_2}{\partial p} \frac{dp}{dt} + V_2 \frac{\partial \rho_2}{\partial h} \frac{dh_2}{dt} \quad (9)$$

from which:

$$\frac{dp}{dt} = \frac{1}{V_2 \frac{\partial \rho_2}{\partial p}} \frac{dM_2}{dt} - \frac{\partial \rho_2 / \partial h}{\partial \rho_2 / \partial p} \frac{dh_2}{dt}. \quad (10)$$

It is noted that the above derivation is based on assumption that the steam volume V_2 is constant. To judge the consequence of this assumption, we transformed Eq. (10) into the form of pressure equation given in the model I (see Eq. (6)). For this purpose, the density is replaced with the specific volume ($v_2 = 1/\rho_2$) and the term dh_2/dt is expressed from the steam energy equation (Eq. (7) for $i = 2$). After these transformations, the above dp/dt equation takes the following form:

$$\frac{dp}{dt} = \frac{\left(h_2 \frac{\partial v_2}{\partial h} - v_2 \right) \frac{dM_2}{dt} - \frac{\partial v_2}{\partial h} [(mh)_{2,in} - m_{2,out}h_2 + m_e h' - m_e h_2]}{\frac{\partial v_2}{\partial p} M_2}. \quad (11)$$

The comparison of Eq. (11) with the corresponding one from the non-equilibrium model I (Eq. (6)) reveals that the terms associated with the liquid phase ($i = 1$) are missing both in the nominator as well as in the denominator. Further, the heat transfer rate due to the temperature difference between phases $Q_{i,TD}$ is also missing in the second term of the nominator.

$$Re_b = \frac{D_b \rho_1 (u_2 - u_1)}{\mu_1}, \quad (21)$$

where μ_1 is the dynamic viscosity of liquid water and the difference $u_2 - u_1$ represents the relative phase velocity. The liquid water may be considered as stagnant ($u_1 = 0$ m/s) and u_2 is approximated by the bubble rise velocity [17]:

$$u_2 = 1.4 \left[\frac{\sigma g (\rho_1 - \rho_2)}{\rho_1^2} \right]^{\frac{1}{4}}, \quad (22)$$

where σ denotes the surface tension and g stands for the gravity. The bubble diameter is evaluated according to [16]:

$$D_b = \frac{We_{cr}\sigma}{\rho_1 (u_2 - u_1)^2} \quad (23)$$

adopting the value of critical Weber number $We_{cr} = 1.24$. The interfacial area concentration is computed as:

Table 3

Non-equilibrium model III- governing equations.

Terms in energy balance equation presented in form of Eq. (A7)				
L ₁	R ₁	R ₂	R ₃	R ₄
$\frac{d(Mu)_i}{dt} = Q_{i,wall} + \phi_{i,PT} + 0 + \phi_{i,in} - \phi_{i,out}$				(12) [15]

Analysis:

The authors use internal energy u as relevant energy balance quantity. Further, the energy flow rates $\phi = mh$ are used for the flows at boundaries (inlet, outlet) and at the phase interface (condensation, evaporation). The term R₁ accounts for the heat transfer rate between liquid water/steam and surrounding PCM envelope (denoted as $Q_{i,wall}$) and for the heat transfer rate due to phase transition $\phi_{i,PT} = (-1)^{i+1}(\phi_c - \phi_e)$.

The comparison with Eq. (A7) shows that the term R₂ i.e. $-p \frac{dV_i}{dt}$ is missing. In relation to that, the energy balance equation is incomplete. The authors state that m_e and m_e are evaluated by closure laws given in [2], but an inspection of the presented formulations shows significant disagreement as discussed in Section 2.1.2.1.

Derivation of differential equation for dp/dt is not presented. Moreover, it is not clear how the pressure change with time dp/dt is formulated as no term including pressure p can be found in presented governing equations. Nevertheless, the authors obtained correct pressure evolution when the model was validated with data given in [2]. Finally, the mass balance equation is incorrect since the mass flow rate m instead of the mass M is used as balance quantity (the term on the l.h.s. of corresponding equation). To summarize, this model cannot be assessed due to the above presented uncertainties.

$$a_{21} = n \left[4\pi \left(\frac{D_b}{2} \right)^2 \right], \quad (24)$$

where the concentration of bubbles is predicted by adjusting analytical relation developed for the adiabatic evaporation in nozzle flow [16,18] and by adopting the value 6.8 (instead of 12.5) for the free term in the exponent as presented below:

$$n = 10^{6.8 - 0.15 \log Gi}. \quad (25)$$

The parameter Gi is evaluated from:

$$Gi = \frac{16\pi\sigma^3}{3k_B r^2 T_1 (h_1/h' - 1)^2 \rho'^2}, \quad (26)$$

where k_B represents the Boltzmann constant ($k_B = 1.38 \cdot 10^{-23}$ J/K).

Applying the above methodology to the case of charging an industrial steam accumulator in a coal drying plant (for the accumulator geometry see Table 6, for the charging conditions see Fig. 4) Stevanovic et al. [3] obtained values of τ_c slightly lower than the empirical value $\tau_c = 85$ s. The pressure evolution computed with these values of τ_c agrees well with measured data.

In the non-equilibrium model II the evaporation and condensation rates are evaluated as:

$$m_e = \frac{M_1(h_1 - h') + m_{1,in}(h_{1,in} - h')}{h'' - h_1} \quad \text{for } h_1 > h' \quad (27)$$

$$m_c = \frac{M_1(h' - h_1) + m_{1,in}(h' - h_{1,in})}{h'' - h'} \quad \text{for } h_1 < h'. \quad (28)$$

The comparison of the above expressions for m_e and m_c with those used in the non-equilibrium model I (see Eqs. (14) and (15)) shows the following. Different to the non-equilibrium model I, in the non-equilibrium model II (i) the energy inflow of the liquid water $m_{1,in}h_{1,in}$ is accounted for and (ii) no relaxation factors τ_e and τ_c are implemented in relations (27) and (28).

As presented in Table 3, Niknam and Sciacovelli [15] state that the mass flow rate due to phase transition is determined by methodology applied in the non-equilibrium model I, i.e. by approach presented in [3]. However, we could find significant inconsistencies, which are here noted. Using the original notation from Niknam and Sciacovelli [15], the

Table 4

Non-equilibrium model IV - governing equations.

Terms in energy balance equation presented in form of Eq. (A8)					Eq.	Applied in:
L ₁	R ₁	R ₂	R ₃	R ₄		
$\frac{d(Mh)_i}{dt} =$	$Q_{i,TD} + (mh)_{i,PT}$ $- Q_{i,wall}$	$+ V_i \frac{dp_i}{dt}$ $+ p_i \frac{dV_i}{dt}$	$+ m_{i,in} h_{i,in}$	$- m_{i,out} h_{i,out}$	(13)	[6]
Analysis:						
The comparison with Eq. (A8) shows that expression for the term R ₂ includes an abundant term $p_i dV_i/dt$, what makes the energy balance equation (Eq. (13)) incorrect. Further, although in Fig. 2 of their paper the authors show that one value of pressure is prevailing in the entire steam accumulator, in corresponding energy balance equation (see Eq. (13)) the pressure is introduced for each phase separately, that is incorrect. Probably, this is typing error, otherwise there would not be enough equations to close the system. In expression for the term R ₁ there are also some inconsistencies. Therefore, the energy rate due to phase transition is formulated as $(mh)_{i,PT} = (-1)^{i+1} (m_e h' - m_e h)$, i.e. the term $m_e h'$ is given instead of $m_e h''$. This could be another typing error, or maybe the difference between these two terms is included in term $Q_{i,TD}$. The latter could not be checked as no expression for $Q_{i,TD}$ is given. Finally, the term R ₁ includes the heat rate transferred to the walls of steam accumulator vessel $Q_{i,wall}$, but the way how $Q_{i,wall}$ is evaluated, is not presented. As none of the closure laws is given, the above statements about the typing errors could not be checked directly.						
Derivation of differential equation for dp/dt is not given. Nevertheless, an indirect confirmation could be done as the authors presented validation of the model with experimental data from [2]. This situation indicates that the abundant term $p_i dV_i/dt$ contributes little to the enthalpy change. This may be true, especially in case of the liquid phase because very large changes of mass are necessary to cause small changes of volume. To summarize, this model includes incorrect terms. Therefore, as neither the final form of governing equations nor the closure laws are presented, the model could not be assessed.						

Table 5

Test conditions used for estimation of relaxation factor.

Steam accumulator type	V(m ³)	Initial pressure p_0 (bar)	Steam accumulator transient	Steam flow rate (kg/s)	Thermal state of charging/discharged steam	τ_c (s)	τ_e (s)
Estimated by Stevanovic et al. [2] and used in [3,5,7,15]							
Industrial steam accumulator in coal drying plant	64	34	Charging	Variable in time, see Fig. 4	Variable in time, see Fig. 4	85	–
Estimated by Sun et al. [4]							
Lab-type steam accumulator	1.12	6.5	Charging	0.2	$p_{2,in} = 0.663 \text{ MPa}$ $T_{2,in} = 280.2 \text{ }^\circ\text{C}$	9.1	–
		6.5	Charging	0.25	$p_{2,in} = 0.8 \text{ MPa}$ $T_{2,in} = 268.9 \text{ }^\circ\text{C}$	8.0	–
		12	Charging	0.21	$p_{2,in} = 1.39 \text{ MPa}$ $T_{2,in} = 293.7 \text{ }^\circ\text{C}$	9.5	–
		11.5	Discharging	N/A	saturated (function of p in steam accumulator)	–	1.0
		5.9	Discharging	N/A	saturated (function of p in steam accumulator)	–	1.4

mass transfer due to evaporation/condensation is given by:

$$m = \phi / h_{sat}, \quad (29)$$

where

$$\phi = M(h - h_{sat}) / \tau. \quad (30)$$

We note the following. Even when in the above relations M is replaced with M_1 , h with h_1 , h_{sat} with h' and τ with τ_e , Eq. (14) for the evaporation mass rate used in the non-equilibrium model I cannot be obtained as h' is used in the denominator instead of r . In case of condensation, transformed Eqs. (29) and (30) show even less similarity with Eq. (15).

Here presented equations for the prediction of the evaporation and condensation mass transfer rates during steam accumulator pressure transients under non-equilibrium thermal conditions (Eqs. (14)–(15)),

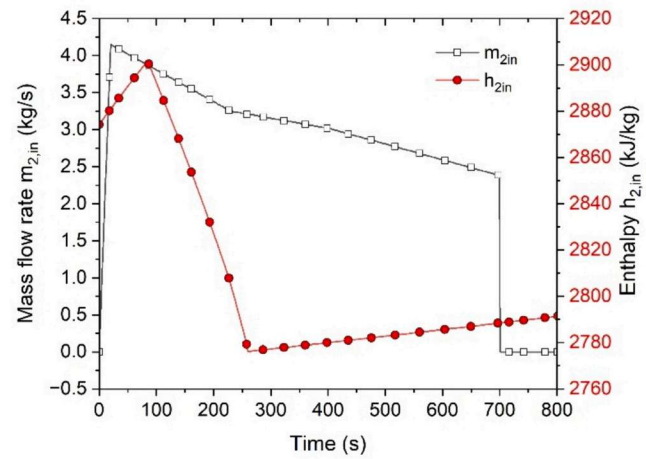


Fig. 4. Charging conditions for the benchmark case. Mass flow rate and enthalpy of inflow steam are adopted from [2].

Table 6

Geometrical and material data of steam accumulator reported by Stevanovic et al. [2].

Inner volume, V	64 m ³	Outer diameter, D_o	2.8 m
Outer volume, V_o	72.31 m ³	Wall thickness, δ	0.083 m
Volume of vessel walls, V_{wall}	8.27 m ³	Inner diameter, D	2.63 m
Total length, L	11.9 m	Mass of vessel walls, M_{wall}	$6.49 \cdot 10^4$ kg
Specific heat of vessel walls, c_{wall}	420 J/kgK	Heat capacity of vessel walls	$2.73 \cdot 10^7$ J/K

(27)–(28) and (29)) are empirical. The potential for the mass transfer is calculated as the enthalpy difference: $(h_1 - \bar{h})$ in case of evaporation and $(\bar{h} - h_1)$ in case of condensation. The influence of the interfacial area concentration and the heat transfer at the steam-liquid water interface on the phase transition rate are included through the relaxation factors τ_e and τ_c respectively for the evaporation and condensation. A theoretical approach to the determination of relaxation factors is presented with the derivation outlined with Eqs. (16)–(26), but this derivation is also based on the empirical correlations for the interface heat transfer (Eq. (20)), for the calculation of the steam bubble diameter (Eq. (23)) and the prediction of concentration of steam bubbles (Eq. (25)). Obviously, in-depth prediction of the interfacial geometry and concentration and the heat transfer at the phase interface under laminar and/or turbulent steam and liquid water relative flows would require complex three-dimensional simulations with the computational fluid dynamics methods and numerical interface tracking, which is beyond practical engineering computations. Therefore, from the engineering point of view, it was found both reliable and practical to apply the correlations in the form of Eqs. (14) and (15), in which the complex phenomena are expressed through the enthalpy difference, as the potential for phase transition, and through the relaxation factor that accounts for both the interfacial area concentration and the interface heat transfer that supplies heat to the interface for evaporation and removes heat from the interface under condensation.

In addition, for the sake of completeness, it should be mentioned that a number of correlations are reported in the literature for the prediction of phase transition rate at the vapour-liquid interface, mainly with the application to adiabatic evaporation in the hot liquid flashing or to the bubble dynamics in boiling [19]. A review of these correlations is beyond the scope of this paper, but the general approaches can be summarized as the correlations based on the conduction controlled heat transfer at the vapour-liquid interface [22,23], the convection controlled heat transfer at the interface [24], the surface renewal theory [25] or the kinetic theory of gasses analogy [26]. The application of these approaches to the steam accumulator geometry and operating conditions might be the topic of future research.

2.1.2.2. Heat transfer rate due to temperature difference between phases. The heat transfer rate due to the temperature difference between the steam and the liquid water is evaluated as:

$$Q_{21} = h_{21} a_{21} \Delta T_{21} V_1, \quad (31)$$

where $\Delta T_{21} = T_2 - T_1$ when steam is superheated ($T_2 > T_1$) and $\Delta T_{21} = T_1 - T_2$ when liquid water is superheated ($T_1 > T_2$). In majority of publications (for example, [2,4,5,7]) the product of convective heat transfer coefficient and interfacial area concentration (ha)₂₁ is considered as relevant and the value $(ha)_{21} = 50 \cdot 10^3 \text{ W/m}^3\text{K}$ is adopted. In fact, only Stevanovic et al. [3] considered h_{21} and a_{21} as separate variables. While a_{21} is evaluated from Eq. (24), the determination of heat transfer coefficient is based on the theoretical solution for transient conduction in sphere [16]:

$$h_{21} = 16 \frac{\lambda_2}{D_b} \quad (32)$$

where λ_2 represents thermal conductivity of steam.

It should be noted that the heat transfer rate due to temperature difference between liquid water and steam $Q_{TD} \equiv Q_{21}$, calculated with Eq. (31), is a different mechanism from the heat transfer rate due to the phase transition $(mh)_{i,PT}$. Nevertheless, the heat transfer rate Q_{21} can be expressed by the heat transfer rate due to phase transition as follows. The difference of enthalpies Δh in Eqs. (14) and (15) can be expressed as the temperature difference between the saturation temperature and the actual liquid water temperature ΔT by introduction of the enthalpy and temperature relation $\Delta h = \bar{c}_{p,1} \Delta T$, where $\bar{c}_{p,1}$ is the mean value of the

isobaric specific heat for liquid water, averaged for the temperature range ΔT . The heat transfer rate due to the phase transition is expressed as:

$$(mh)_{i,PT} = \frac{\rho_1 V_1 \bar{c}_{p,1} \bar{h}' \Delta T}{\tau_e r}. \quad (33)$$

The relaxation factor is derived from Eqs. (18) and (19) and with the introduction of $\Delta h = \bar{c}_{p,1} \Delta T$ in Eq. (18), the following form is obtained:

$$\tau_e = \frac{\rho_1 \bar{c}_{p,1}}{a_{21} k_{1,int}} \quad (34)$$

Introduction of Eq. (34) into Eq. (33) leads to:

$$(mh)_{i,PT} = \frac{a_{21} k_{1,int} \bar{h}' V_1}{r} \Delta T \quad (35)$$

From the ratio of Eqs. (31) and (35) follows:

$$Q_{21} = \frac{h_{21} r}{k_{1,int} \bar{h}'} (mh)_{i,PT} \quad (36)$$

From relation (36) and taking into account Eqs. (20) and (32) for the calculation of $k_{1,int}$ and h_{21} respectively, it can be concluded that Q_{21} is an order of magnitude lower than $(mh)_{i,PT}$. Introduction of Eqs. (20) and (32) into Eq. (36) leads to:

$$\frac{Q_{21}}{(mh)_{i,PT}} = \frac{16 \lambda_2 r}{\lambda_1 (2 + 0.74 Re_b^{1/2} Pr_1^{1/3}) \bar{h}''} \quad (37)$$

For illustration, the ratio of $Q_{21}/(mh)_{i,PT}$ is estimated, for instance, at 30 bar. The saturated liquid water and steam thermal conductivities are respectively $\lambda_1 = 0.638 \text{ W/(mK)}$ and $\lambda_2 = 0.047 \text{ W/(mK)}$, the latent heat is $r = 1794.9 \text{ kJ/kg}$ and the saturated steam enthalpy is $\bar{h}'' = 2803.3 \text{ kJ/kg}$. The value of the product $0.74 Re_b^{1/2} Pr_1^{1/3}$ depends on the bubble Reynolds number, and without further analysis of the bubbling hydrodynamics, i.e. assuming that the bubble is stagnant in relation to the surrounding liquid water, it can be concluded that at least $\frac{Q_{21}}{(mh)_{i,PT}} < \frac{16 \cdot 0.047 \cdot 1794.9}{0.638 \cdot 2803.3} = 0.38$.

The simulation of the steam accumulator experimental conditions indicates that the above ratio is even lower. Here an example is given for the case of charging of large steam accumulator. The results of corresponding simulation presented in Section 4.1.2 show that $Q_{21} \sim 150 \text{ kW}$ (see Fig. 11c), while the condensation rate is about $m_c \sim 3.5 \text{ kg/s}$ (see Fig. 11b) at time instant 200 s. Multiplying m_c with the corresponding saturated steam enthalpy ($\bar{h}'' \sim 2800 \text{ kJ/kg}$) results in $(mh)_{i,PT} \sim 9800 \text{ kW}$ and gives the ratio $Q_{21}/(mh)_{i,PT} \sim 0.015$.

2.2. Equilibrium model of steam accumulator dynamics

In equilibrium models, both phases are assumed to be in thermal equilibrium, i.e. saturated. For this state, the specific enthalpy of steam-liquid water mixture in the steam accumulator can be evaluated as:

$$h = \bar{h} + x(\bar{h}' - \bar{h}'), \quad (38)$$

where the quality x is expressed using the specific volume $v = V/M$:

$$x = \frac{v - v'}{v' - v''} \quad (39)$$

As the two-phase mixture is thermally homogeneous, neither mass nor heat transfer over the phase interface takes place ($m_e = m_c = 0$ and $Q_{21} = 0$). Therefore, the mass balance equation is given by:

$$\frac{dM}{dt} = m_{1,in} - m_{1,out} + m_{2,in} - m_{2,out}, \quad (40)$$

while the energy conservation is expressed as:

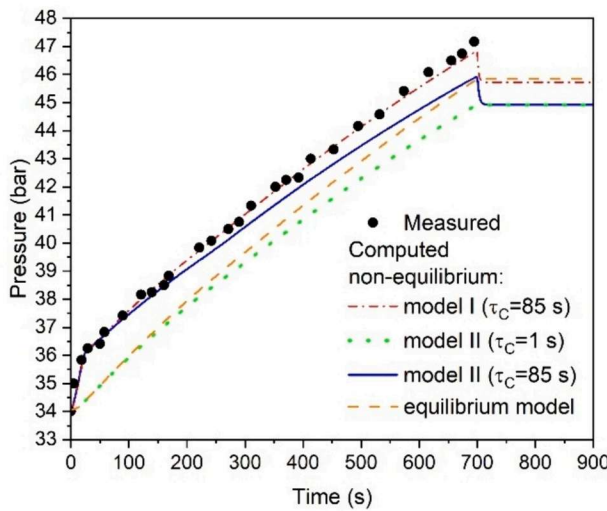


Fig. 5. Comparison of measured and pressure evolution computed by different models for steam accumulator dynamics. Charging conditions and steam accumulator geometry are adopted from [2] (see Fig. 4 and Table 6).

$$\frac{d(Mh)}{dt} = m_{1,in}h_{1,in} - m_{1,out}h' + m_{2,in}h_{2,in} - m_{2,out}h' + V \frac{dp}{dt}. \quad (41)$$

The equation of pressure change with time is derived by taking time derivatives of the enthalpy of two-phase mixture $H = Mh$, of the specific enthalpy h and of the quality x and substituting them into Eq. (41):

$$\frac{dp}{dt} = \frac{m_{1,in}h_{1,in} - m_{1,out}h' + m_{2,in}h_{2,in} - m_{2,out}h' + \left(\frac{rv}{v'-v} - h\right)(m_{1,in} - m_{1,out} + m_{2,in} - m_{2,out})}{M \left(\frac{dh'}{dp} + \frac{v-v'}{v'-v} \frac{dr}{dp} - \frac{r}{v'-v} \frac{dv'}{dp} - r \frac{v-v'}{v'-v} \frac{d(v''-v')}{dp} \right) - V}. \quad (42)$$

For more details on this derivation, see [3].

Eqs. (40) and (42) represent governing equations of the equilibrium model. Solving these equations for given initial conditions $M(t = 0)$ and $p(t = 0)$ enable numerical computations of the steam accumulator dynamics - knowing M provides evaluation of x and knowing p provides determination of temperature and all other properties of saturated phases (such as specific enthalpy, specific volume, etc.). No closure laws are needed in this model.

3. Assessment of governing equations

Section 2 presents different forms of the governing equations for the modelling of two-phase steam-liquid mixture dynamics within steam accumulators. In this Section, the performance of these equations is assessed. As presented in Table 3, the non-equilibrium models denoted by III (Niknam and Sciacovelli [15]) and by IV (Richter et al. [6]) are associated either with insufficient data or incorrect terms in corresponding governing equations. Therefore, an attempt to assess the performance of models III and IV would not be reasonable. In relation to that, this Section deals with the governing equations of the non-equilibrium models I and II (presented in Tables 1 and 2). In addition, the performance of the equilibrium model is appraised. For that purpose, the charging transient of the steam accumulator described by Stevanovic et al. [2] is used as the benchmark case. The geometrical and material data of the accumulator are given in Table 6, while the mass flow rate $m_{2,in}$ and the enthalpy $h_{2,in}$ of charging steam are presented in Fig. 4.

3.1. Results for bare steam accumulator

The performance of considered models is assessed by comparison of measured data for pressure with computational results for the case of a bare steam accumulator. The term “bare” means that the two-phase steam-liquid water system within the steam accumulator is perfectly thermally insulated, i.e. that the heat transfer rate to the walls of steam accumulator vessel $Q_{i,wall}$ is neglected.

The non-equilibrium model I was run adopting values $\tau_c = 85$ s for the relaxation factor of condensation mass rate and $(ha)_{21} = 5 \cdot 10^4$ W/m³K for interfacial heat transfer rate per unit liquid volume and temperature difference of 1 K. Regarding the non-equilibrium model II, we note the following. As in the considered charging test there is no water inflow ($m_{1,in} = 0$ kg/s), the closure assumption for the steam condensation rate m_c reduces to the form of the one applied in the model I: the difference $h' - h_1$ in the non-equilibrium model II is close to r in the model I and relaxation factor $\tau_c = 1$ s can be formally introduced in the model II. This reduction gives the possibility to assess the consequences of omitted terms in balance equations of model II (see discussion in Table 2) in the following way. Therefore, when the value $\tau_c = 85$ s is adopted in the model II, the value of m_c is close to the one in model I. This means that the observed differences between performance of models I and II can be solely related to the terms missing in the model II.

The obtained results are presented in Fig. 5, where the pressure evolution computed by the non-equilibrium models I and II as well as by the equilibrium model is compared with corresponding measured data. Fig. 5 shows that pressure computed with the non-equilibrium model I agrees well with measured data during the whole duration of the transient. The pressure curve evaluated by the equilibrium model un-

derestimates the intensive pressure increase at the beginning of the transient (time $t < \sim 50$ s) when the non-equilibrium effects associated with the interfacial mass and the heat transfer are pronounced. For $t > \sim 50$ s this curve is almost parallel to the one obtained by the non-equilibrium model I. After the charging of steam accumulator is stopped, the pressure computed with the equilibrium model overlaps with the one obtained by the non-equilibrium model I. Therefore, it may be stated that the governing equations of the equilibrium model are not suitable for an accurate prediction of the transient behaviour of the steam-liquid water system within the steam accumulator in cases when the non-equilibrium effects are pronounced.

As presented in Fig. 5 the pressure evolution computed by the non-equilibrium model II with original closure assumption ($\tau_c = 1$ s) shows significant disagreement with measured data – the disagreement increases during the course of transient. Moreover, after the charging is stopped, the pressure value computed by the model II is lower than the one obtained by the equilibrium model and by the non-equilibrium model I. The situation is something different when the value $\tau_c = 85$ s is applied in closure assumption for m_c in the non-equilibrium model II. Therefore, for $t < \sim 200$ s the agreement with measured data is good, meaning that the value of m_c governs the evolution of pressure at the beginning of transient. However, for $t > \sim 200$ s the pressure curve evaluated with this model increasingly deviates from the measured data. At the end of transient, the pressure is underestimated in comparison with the measured one in the same extent as by the non-equilibrium model II with the original closure assumption ($\tau_c = 1$ s). Therefore, it may be stated that such incorrect behaviour of the pressure curve is due

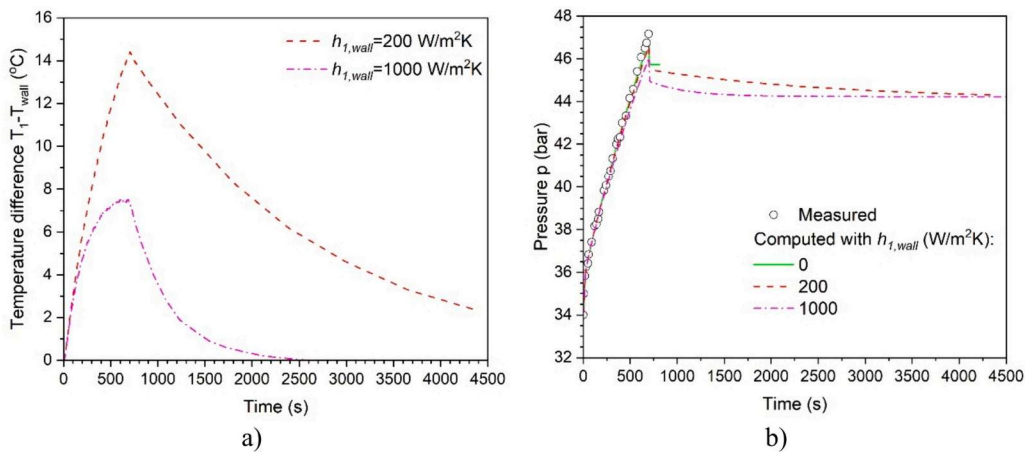


Fig. 6. Accounting for the effect of heat transfer to the walls of steam accumulator vessel: (a) temperature difference between liquid and vessel walls and (b) evolution of steam accumulator pressure. Charging conditions and steam accumulator geometry are adopted from [2] (see Fig. 4 and Table 6).

to the missing terms in the balance equations of non-equilibrium model II. This means that the governing equations in the non-equilibrium model II cannot correctly describe the dynamics of two-phase mixture in the steam accumulator.

Based on the aforementioned, it is to conclude that only the governing equations of the non-equilibrium model I are suitable for the prediction of the steam accumulator dynamics. In relation to that, this model is going to be exposed to further examination in next Sections. The examinations are related to the term which accounts for the heat transfer to the walls of steam accumulator vessel (addressed in Section 3.2) and the applicability of closure laws to accumulators of different geometry and different transient conditions (addressed in Section 4).

3.2. Effects of heat transfer to the walls of steam accumulator vessel

Before the transient starts, the walls of steam accumulator vessel are at the temperature equal to the saturation temperature for the accumulator initial pressure p_0 . In the case of here considered charging transient $T_{wall,0} = T_{sat}(p_0) = 240.98 \text{ }^\circ\text{C}$. During the transient, the temperature of two-phase water system within the steam accumulator increases in accordance with the pressure increase. For reference, the temperature increase of two-phase mixture after the transient end is $\Delta T \sim 18 \text{ }^\circ\text{C}$. This gives the temperature increase rate of $\sim 1.54 \text{ }^\circ\text{C/min}$. Assuming that the heat transfer to the walls of steam accumulator vessel takes place by free convection, the heat transfer coefficient has rather low values: $h_{1,wall} = 200\text{--}2000 \text{ W/m}^2\text{K}$ for the liquid water and $h_{2,wall} = 20\text{--}100 \text{ W/m}^2\text{K}$ for the steam. Taking into account these conditions as well as the large mass of vessel walls ($M_{wall} = 6.49 \cdot 10^4 \text{ kg}$, see Table 6), it is of importance to check whether the heat transfer rate to the vessel walls, Q_{wall} , affects the steam accumulator dynamics.

The mechanisms of heat transfer to the vessel walls are implemented in governing equations of the non-equilibrium model I in the following way. The term R_1 in energy Eq. (1) is extended by the heat rate transferred from phase i to walls of steam accumulator $Q_{i,wall}$, i.e. $R_1 = Q_i \cdot TD + (mh)_{i,PT} \cdot Q_{i,wall}$ and $Q_{i,wall}$ is expressed for each phase i ($i = 1, 2$) as:

$$Q_{i,wall} = h_{i,wall} A_{i,w} (T_i - T_{wall}), \quad (43)$$

where $A_{i,w}$ represents a portion of surface of inner vessel wall wetted by phase i . In this paper, the surface $A_{i,w}$ is determined from the computed liquid level and the known steam generator geometry. Further, in Eq. (43) it was assumed that the whole vessel wall is at the volume averaged temperature T_{wall} . Therefore, the wall temperature T_{wall} can be evaluated when the following balance equation is implemented in the non-equilibrium model I:

$$\frac{d(Mc_p T)_{wall}}{dt} = Q_{wall} - Q_{atm}, \quad (44)$$

where $Q_{wall} = Q_{1,wall} + Q_{2,wall}$ and $Q_{atm} = Q_{1,atm} + Q_{2,atm}$ represents the losses through thermal insulation ($Q_{i,wall}$ and $Q_{i,atm}$ are denoted in Fig. 3).

The computations were done for two values of heat transfer coefficient from the liquid water to vessel walls: the low one ($h_{1,wall} = 200 \text{ W/m}^2\text{K}$) and the moderate one ($h_{1,wall} = 1000 \text{ W/m}^2\text{K}$). For the heat transfer coefficient from steam to vessel wall the value $h_{2,wall} = 20 \text{ W/m}^2\text{K}$ is adopted. As the purpose of this investigation is to estimate the effect of heat transfer to the vessel wall from the fluid inside the steam accumulator, the heat losses through the insulation Q_{atm} are neglected. Taking into account that $h_{1,wall}$ is at least one order of magnitude higher than $h_{2,wall}$, the heat transferred from the liquid water to the vessel walls is dominant and the temperature difference $T_1 - T_{wall}$ may be considered as relevant. Fig. 6a shows that this temperature difference increases during the whole transient, but then decreases after the charging stops. The rate of increase/decrease of difference $T_1 - T_{wall}$ is larger for a lower value of heat transfer coefficient $h_{1,wall}$.

The corresponding pressure evolution is presented in Fig. 6b. For reference, the results with neglected Q_{wall} (denoted with $h_{1,wall} = 0 \text{ W/m}^2\text{K}$) are also shown. Fig. 6b shows that accounting for Q_{wall} leads to something lower pressure values in comparison to the measured data. This discrepancy is slight when $h_{1,wall} = 200 \text{ W/m}^2\text{K}$. When $h_{1,wall} = 1000 \text{ W/m}^2\text{K}$ the computed pressure is notably lower at the transient end ($\sim 0.8 \text{ bar}$ at $t = 700 \text{ s}$). However, the following is important to observe - in case when Q_{wall} is accounted for, the pressure curve does not take a constant value after the transient end, but continues to fall down because the heat transfer to the vessel wall takes place as long as there is a temperature difference between the liquid water and the wall (see Fig. 6a). For the example considered here, the pressure computed with $h_{1,wall} = 1000 \text{ W/m}^2\text{K}$ is $\sim 1.5 \text{ bar}$ lower when the steady state is reached ($t > 3000 \text{ s}$) than in case when Q_{wall} is neglected. In case $h_{1,wall} = 200 \text{ W/m}^2\text{K}$ the pressure decrease is slower. Nevertheless, in the steady state it will reach similar value as in case $h_{1,wall} = 1000 \text{ W/m}^2\text{K}$ as can be drawn

Table 7

Overview of steam accumulators for which measured data are available.

	Stevanovic et al. [2]	Sun et al. [4]	Kasper et al. [14]
Volume, $V (\text{m}^3)$	64	1.12	0.88
Inner diameter, $D (\text{m})$	2.5	0.776	0.686
Type	Industrial	Lab	Lab
Classified as steam accumulator with	Large volume	Small volume	Small volume
Considered transient	Charging	Charging	Discharging

Table 8

Main parameters of steam accumulator charging for cases presented by Sun et al. [4].

	Case A	Case B	Case C
Pressure of charging steam, $p_{2,in}$ (bar)	6.63	8	13.9
Temperature of charging steam, $T_{2,in}$ (°C)	280.2	268.9	293.7
Mass flow rate of charging steam $m_{2,in}$ (kg/s)	0.2	0.25	0.21
Initial pressure, p_0 (bar)	4.84	4.84	8.62
Set pressure for closing of steam accumulator charging, p_s (bar)	6.5	6.5	12
Content of liquid phase, V_l/V (-)	0.45	0.52	0.35
Relaxation factor, τ_c (s)	9.1	8	9.5

from Fig. 6b.

Therefore, it is to conclude, that the heat transfer to the vessel walls may play significant role during the transient as well as after the transient end. The latter is important because it will cause pressure decrease after the steam accumulator was charged and is in stand-by mode. The rate of pressure decrease depends on the mass of vessel walls M_{wall} and on the heat transfer coefficient $h_{l,wall}$.

4. Assessment of closure laws

This Section deals with the performance of closure laws applied in the non-equilibrium model I. First, the relaxation factors τ_c and τ_e involved respectively in the evaluation of the condensation and evaporation rate (see Eqs. (14) and (15)) are assessed. These investigations are presented in Section 4.1. Next, the closure law for the heat transfer rate due to temperature difference between phases Q_{21} (see Eq. (31)) is analyzed. The results obtained for the representative transient case are discussed in Section 4.2.

At this place, we would like to point out that experimental investigations of the steam accumulator transients are scarce. In fact, only three publications report measured data related to steam accumulator charging/discharging: Stevanovic et al. [2] present data on an industrial type steam accumulator, while Sun et al. [4] and Kasper et al. [14] deal with lab-type steam accumulators. The investigation presented in this Section is based on the measured data from these experiments. The main characteristics of considered steam accumulators are presented in Table 7.

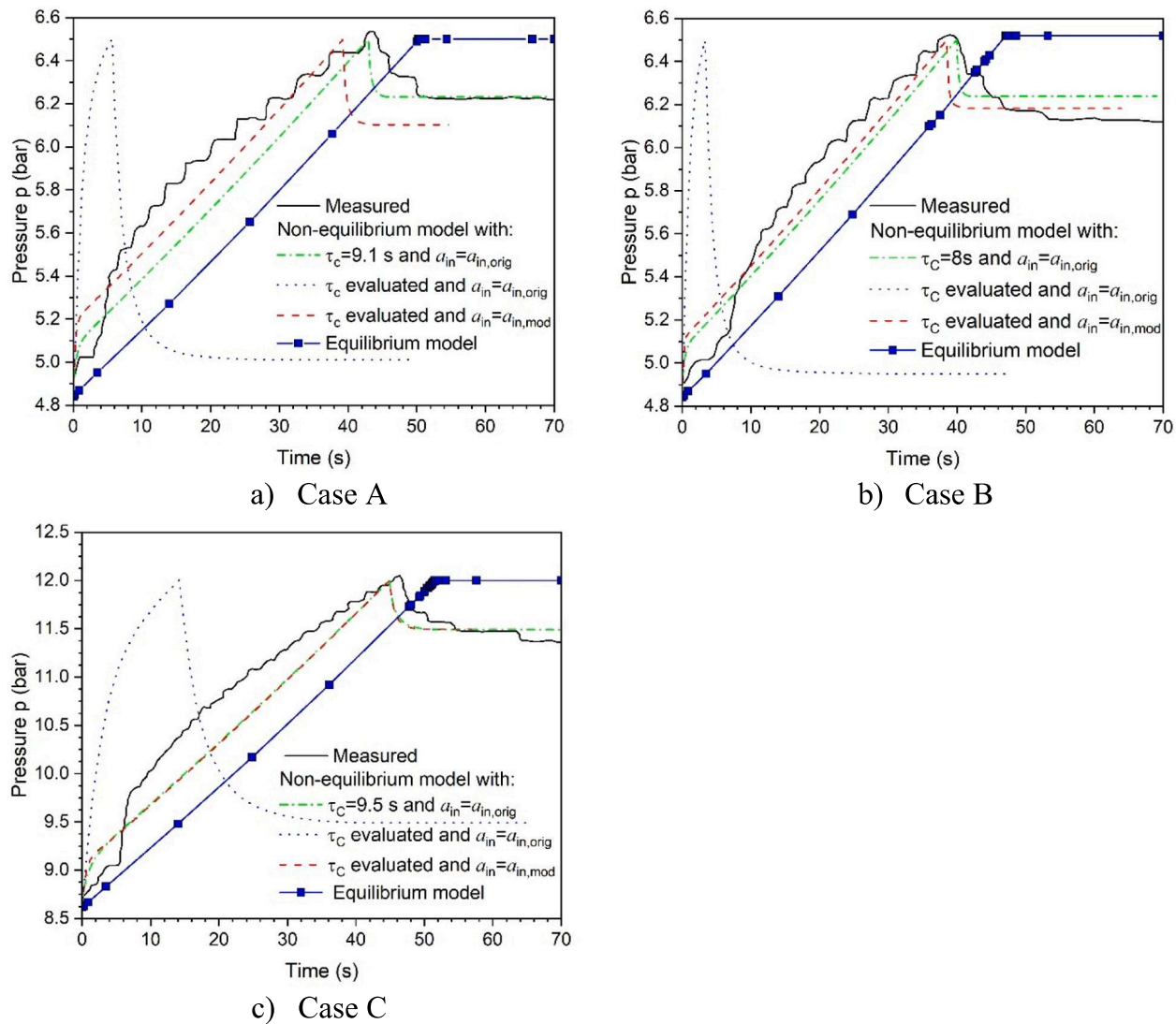


Fig. 7. Comparison of computed and measured pressure evolution during charging of steam accumulator with small volume. Charging conditions and geometry of the steam accumulator are adopted from [4] (see Table 8). (For interpretation of the references to colour in this figure, the reader is referred to the web version of this article.)

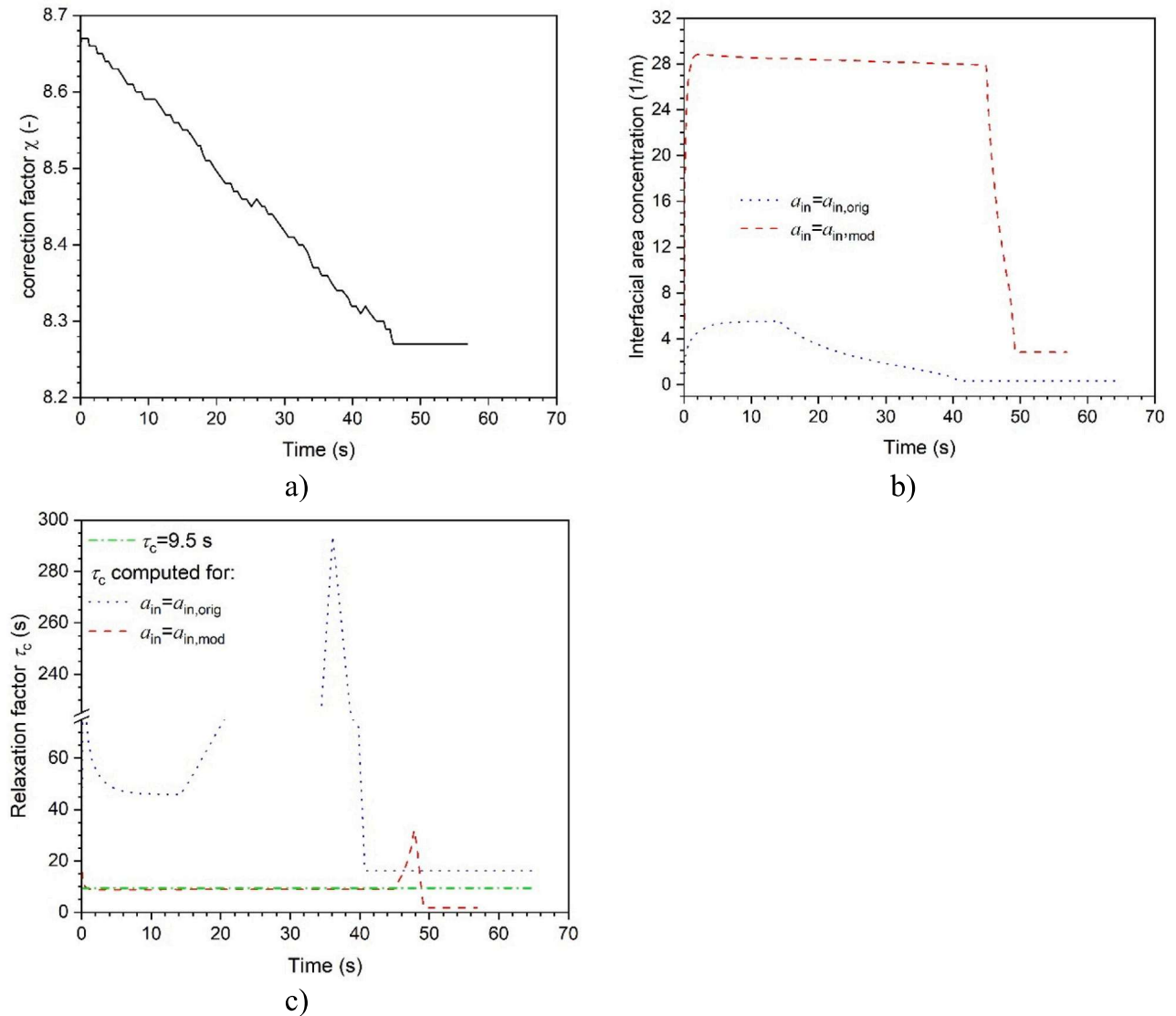


Fig. 8. Correction factor χ (graph a) and effect of its implementation on interfacial area concentration a_{in} (graph b) and relaxation factor τ_c (graph c) in case of charging of steam accumulator with small volume. Evaluations are done for Case C from [4] (see Table 8).

4.1. Evaluation of relaxation factor in closure laws for interphase mass transfer

As discussed in Section 2.1.2, the crucial variable for an accurate evaluation of mass transfer rate during phase change is the relaxation factor τ_i ($i = c, e$). This parameter is mainly evaluated empirically on the bases of experimental data for considered steam accumulator (Stevanovic et al. [2], Sun et al. 2015 [4]). As presented in Table 5, some authors apply the value of relaxation time obtained by Stevanovic et al. [2] to investigate the dynamics of steam accumulators of different geometry, different initial state and different transient conditions [3,5,7,15]. Finally, although the evaluation of τ_c based on theoretical considerations by Stevanovic et al. [3] (see Section 2.1.2.1) performed well for the considered case of steam accumulator charging, further testing is necessary to check its applicability to steam accumulators of different geometry and operating conditions.

In relation to the aforementioned, the goal of this Section is to assess the validity of approaches for the determination of relaxation factor. The assessment was done for cases presented in Table 7: charging of one large and one small steam accumulator and discharging of one small steam accumulator. In the following, the obtained numerical results are

presented and discussed.

4.1.1. Charging of steam accumulator with small volume

Sun et al. [4] presented experimental data for three cases of steam accumulator charging (see Table 8). We note that data on the liquid phase content in the steam accumulator V_1/V (which is input for computations) is not reported in [4], but derived in the following way. Using the available data on the relaxation factor τ_c for each transient, the computations were performed for different values of V_1/V until the measured data for the steam accumulator pressure (presented by solid black line in Fig. 7) are retrieved. Special attention is paid on meeting the set pressure for closing of the stop valve during steam accumulator charging p_s . The values of V_1/V obtained in this way are presented in Table 8. The pressure evolution obtained by applying data for τ_c and V_1/V from Table 8 is presented by the green dot-dash curve in Fig. 7 for all three cases.

Next, computations are performed using relaxation factor τ_c which is evaluated from Eq. (18). The obtained results (see blue dot curve in Fig. 7) show dramatic discrepancy from the measured data as well as from the computational ones with τ_c specified according to Table 8. As seen, the pressure increase is very intensive and reaches the set pressure

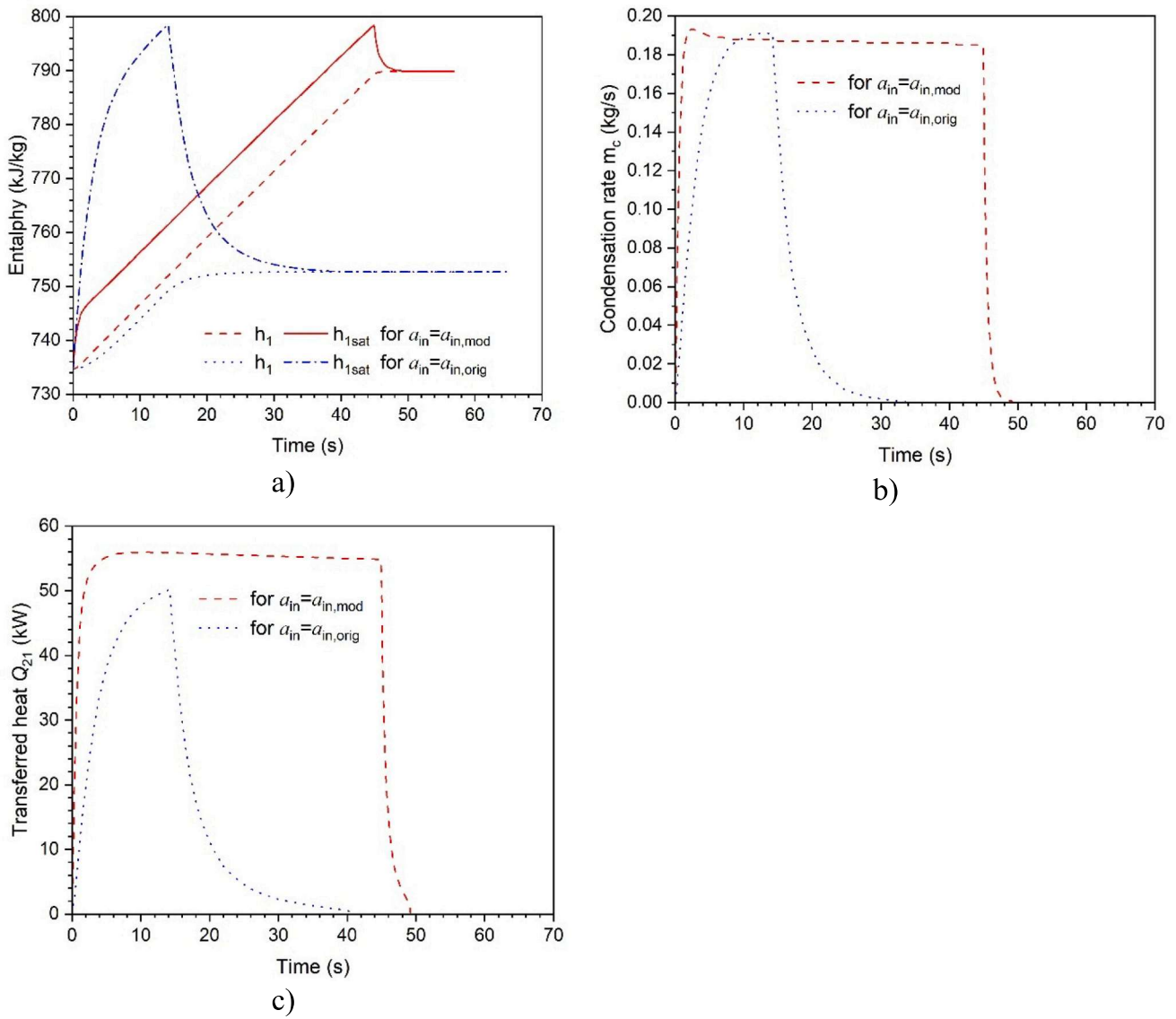


Fig. 9. Effect of modifying interfacial area on main quantities during *charging of steam accumulator with small volume*. Charging conditions and steam accumulator geometry are adopted for Case C from [4] (see Table 8). Corresponding pressure evolution is given in Fig. 7c. (For interpretation of the references to colour in this figure, the reader is referred to the web version of this article.)

p_s after dozens of seconds. This causes the intensive increase of enthalpy of saturated liquid h' (see blue dot dash curve in Fig. 9a). Therefore, the difference $\Delta h_1 = h' - h_1$, which governs condensation rate m_c , increases significantly. Indeed, as presented by the blue dot curve in Fig. 9b, the rate of steam condensation increases massively. This indicates that the value of interfacial area concentration a_{21} , on which phase change occurs, is underestimated by Eq. (24). Following this lead, we introduced the correction factor for interfacial area concentration:

$$\chi = \frac{A_{1,w}}{V_1}, \quad (45)$$

where $A_{1,w}$ denotes the surface of steam accumulator wetted by the liquid phase. Now, the modified interfacial area concentration can be formulated as:

$$a_{in,mod} = \chi a_{in,orig}, \quad (46)$$

where $a_{in,orig}$ represents interfacial area concentration a_{21} computed from its original formulation, i.e. from Eq. (24). For an easier reference, in the text hereafter the interfacial area concentration will generally be

denoted with a_{in} , while the specific cases will be represented as $a_{in} = a_{in,orig}$ or $a_{in} = a_{in,mod}$. The rationale behind the correction factor in the form of Eq. (46) is the influence of the inner surface of steam accumulator vessel walls on the bubble nucleation sites during flashing (accumulator discharge phase), as well as on break up of steam jets and intensity of two-phase mixture circulation during condensation (accumulator charging phase), which is more pronounced in the small volumes than in the large volumes with weak influence of the vessel wall on the bulk two-phase mixture thermohydraulics.

It should be noted that the correction factor χ influences the evaporation and condensation relaxation factors according to Eq. (18), i.e. the relaxation factor depends on the interfacial area concentration that is modified according to Eq. (46). The results that follow in this and Sections 4.1.2 and 4.1.3 demonstrate how the introduction of the correction factor χ influences the relaxation factor, which provides the numerical results for main quantities of various steam accumulator transients in agreement with data measured during steam accumulator transients under laboratory and industrial conditions.

The introduction of correction factor χ i.e. the use of $a_{in,mod}$ leads to immense change of pressure evolution in comparison to the scenario

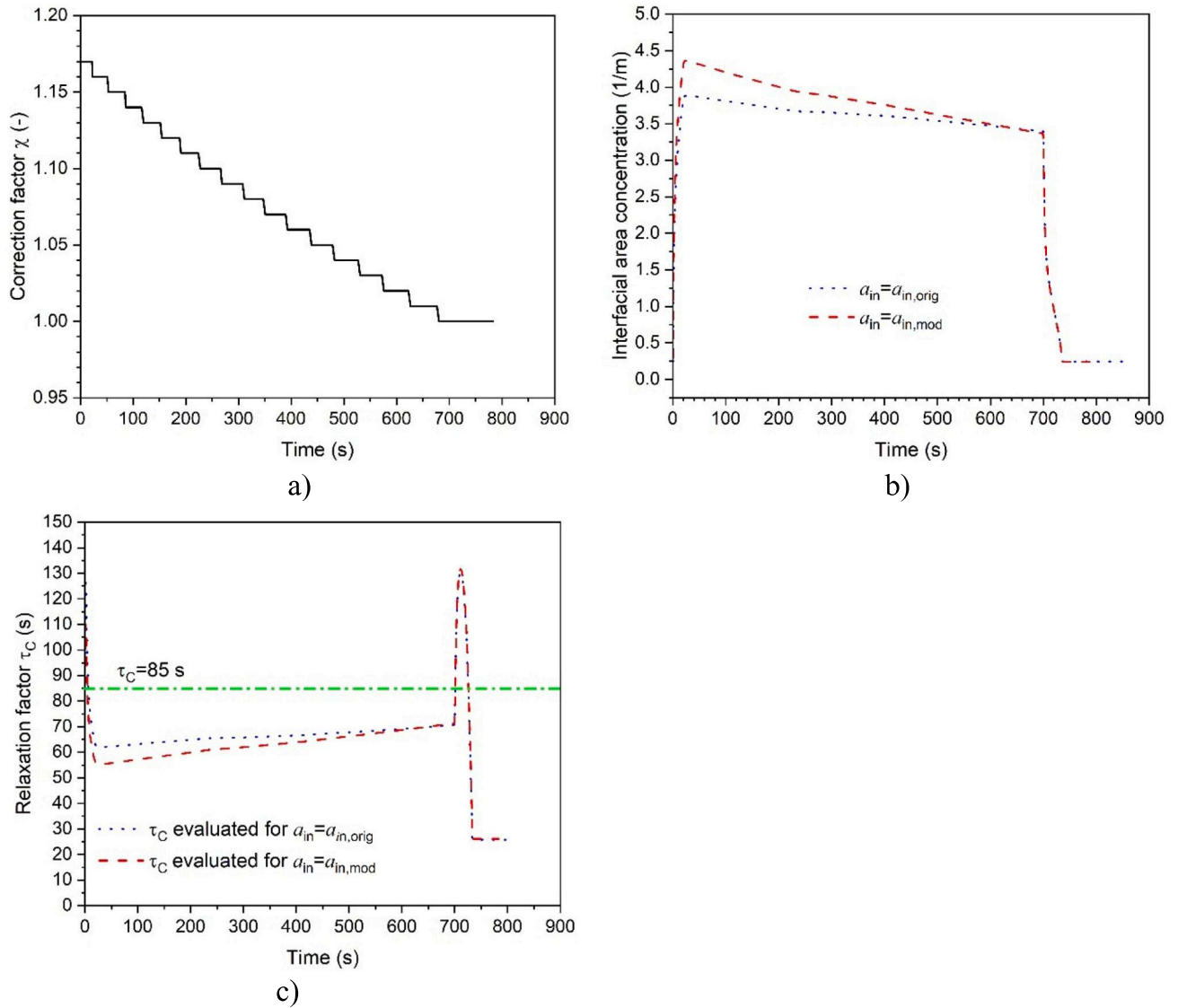


Fig. 10. Correction factor χ (graph a) and effect of its implementation on interfacial area concentration a_{in} (graph b) and relaxation factor τ_c (graph c) in case of charging of steam accumulator with large volume. Charging conditions and steam accumulator geometry are adopted from [2] (see Fig. 4 and Table 6).

when $a_{in} = a_{in,orig}$. This can be observed in Fig. 7 where all three pressure graphs (red dash curves) agree well with measured data when $a_{in} = a_{in,mod}$. The agreement is especially good for Case B and Case C.

To illustrate the effects of the above-implemented modification, we depicted the evolution of correction factor χ and its effect on the interfacial area concentration and relaxation factor in Fig. 8 as well as the evolution of other quantities relevant to steam accumulator transient in Fig. 9. The results obtained for charging of steam accumulator in Case C are presented.

Fig. 8a shows that the correction factor χ slightly decreases, but keeps values $\chi > 8$. Its implementation has a significant effect on the interfacial area concentration as presented in Fig. 8b: $a_{in,mod}$ is higher than $a_{in,orig}$, which leads to more intensive condensation rate m_c at the beginning of the transient and slower increase of pressure p prolonging in that way steam accumulator charging. We note that the sudden change in the character of curves denoted with $a_{in} = a_{in,orig}$ in Fig. 9 is due to the closure of stop valve when the prescribed set point value of maximal pressure is reached during the steam accumulator charging. Therefore, the comparison of corresponding graphs for $a_{in} = a_{in,orig}$ and $a_{in} = a_{in,mod}$ is reasonable only up to this moment. Finally, Fig. 8c shows that the value of relaxation factor τ_c for the case $a_{in} = a_{in,mod}$ almost

overlaps with the value found experimentally ($\tau_c = 9.5$ s). On the other side, τ_c evaluated using $a_{in} = a_{in,orig}$ shows significantly larger values during steam accumulator charging as well as after the stop valve is closed.

Based on the afore-presented considerations it may be stated that in the case of charging of the steam accumulator with small volume, the modification of interfacial area concentration as given by Eq. (46) leads to significant improvement of computational model accuracy.

4.1.2. Charging of steam accumulator with large volume

In the case of the charging transient of the steam accumulator with large volume presented by Stevanovic et al. [2] (see Table 8) only slightly increased values of correction factor χ are observed during the charging transient as presented in Fig. 10a. The introduction of this factor slightly increases the values of interfacial area concentration as shown in Fig. 10b. The relaxation factor τ_c evaluated by applying the modified relation for interfacial area concentration ($a_{in} = a_{in,mod}$) follows the trend of $a_{in} = a_{in,orig}$ graph with something lower values at the beginning of transient (see Fig. 10c). Consequently, the main quantities governing this transient almost overlap for both approaches for the determination of interfacial area concentration as seen in Fig. 11. The

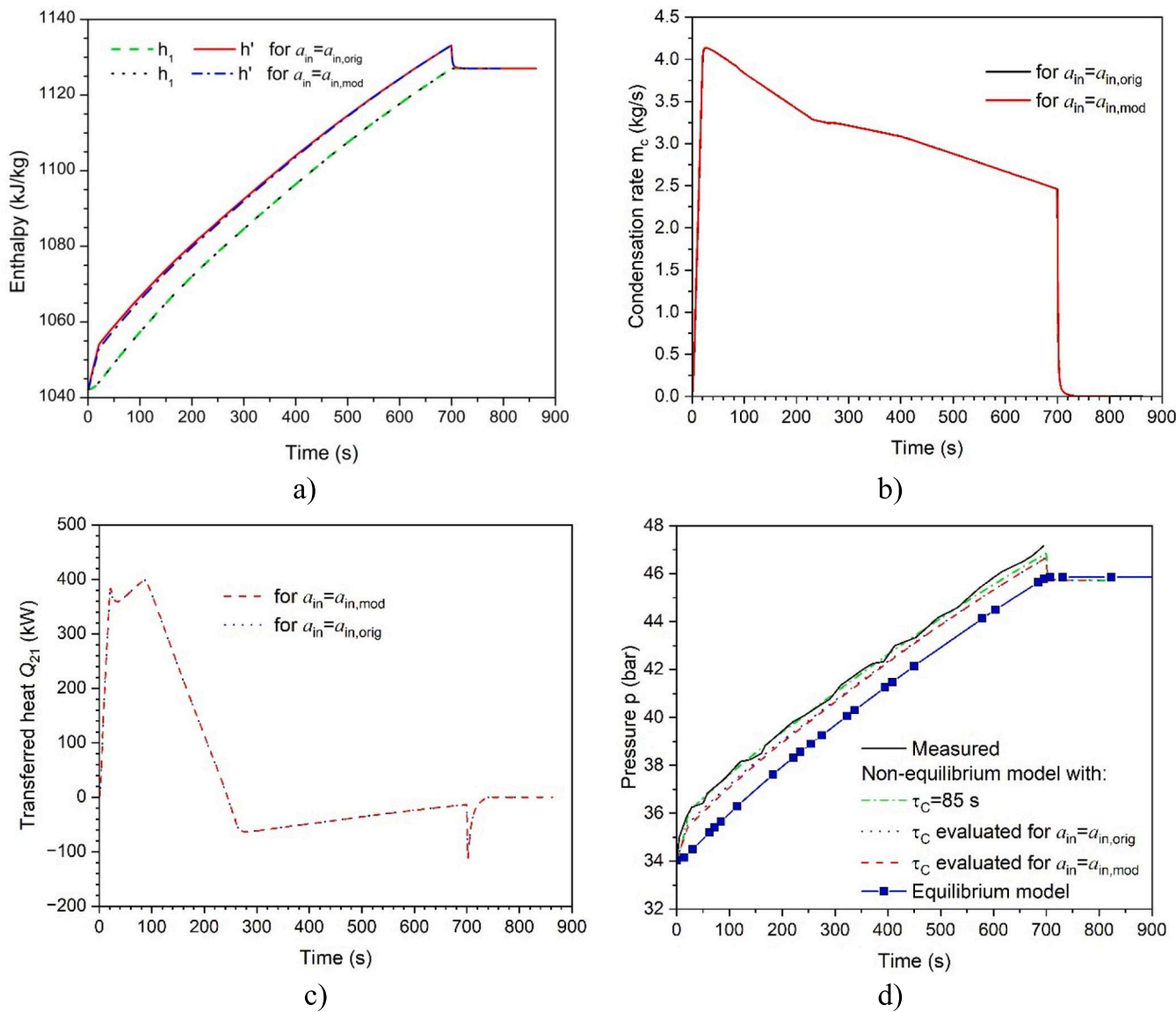


Fig. 11. Effect of modifying interfacial area on the evolution of main quantities during *charging of steam accumulator with large volume*. Charging conditions and steam accumulator geometry are adopted from [2] (see Fig. 4 and Table 6).

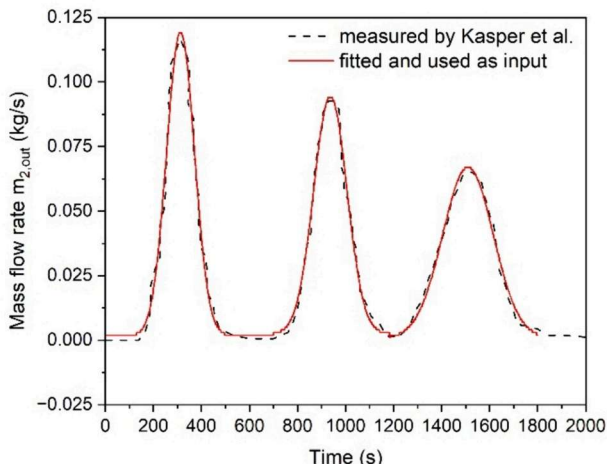


Fig. 12. Mass flow rate of steam during *discharging of steam accumulator with small volume*. Steam accumulator geometry is given in [14] (see Table 7).

pressure evolution obtained for $a_{in} = a_{in,mod}$ is also compared with measured data as well as with results computed applying other numerical approaches in Fig. 11d.

4.1.3. Discharging of steam accumulator with small volume

The experimental data for steam accumulator discharging are presented in two publications: Sun et al. [4] and Kasper et al. [14]. Unfortunately, the paper of Sun et al. [4] does not contain data for the outlet mass flow rate of steam $m_{2,out}$. As $m_{2,out}$ is mandatory input data, these transients could not be modelled. Therefore, this Section deals with the numerical modelling of steam accumulator discharge, experimentally investigated by Kasper et al. [14].

Fig. 12 shows measured data for mass flow rate $m_{2,out}$ given by Kasper et al. [14]. For their application in the numerical model, the data are approximated by three Gaussian like functions as presented by the red solid line in Fig. 12.

Fig. 13a shows that the correction factor χ increases from ~ 3.8 to ~ 4.8 during the transient, that affects values of interfacial area concentration a_{in} (see Fig. 13b) and relaxation factor for evaporation rate τ_e (see Fig. 13c).

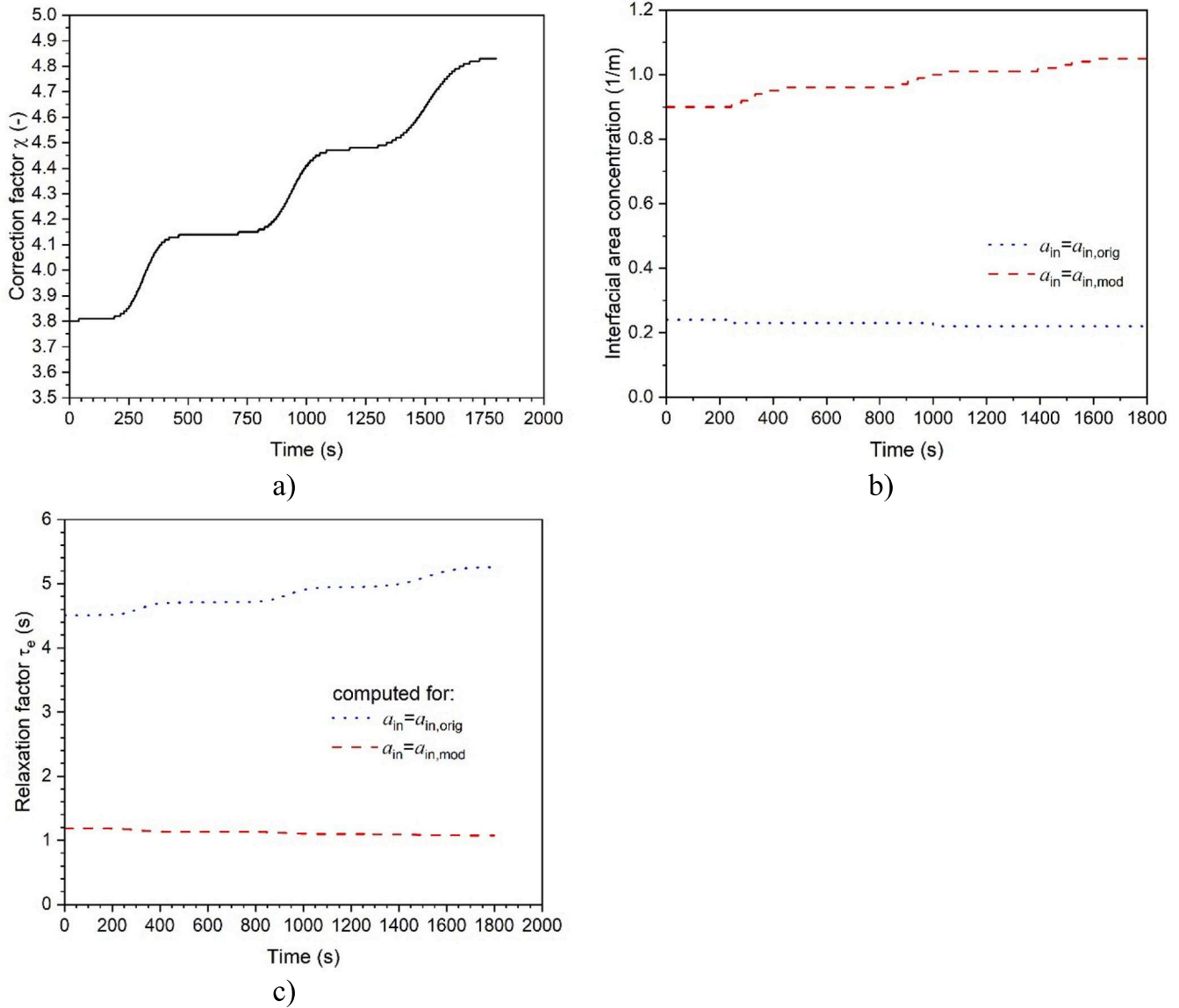


Fig. 13. Correction factor χ (graph a) and effect of its implementation on interfacial area concentration a_{in} (graph b) and relaxation factor τ_c (graph c) in case of discharging of steam accumulator with small volume. Discharging conditions and geometrical data are adopted from [14] (see Fig. 12 and Table 7).

Nevertheless, as seen in Fig. 14b, the implementation of correction factor χ does not influence the evaporation rate m_e . The reason for this is that enthalpy difference $\Delta h_1 = h' - h_1$ is negligible in both cases as can be withdrawn from Fig. 14a. Fig. 14c shows further that the heat transfer rate due to temperature difference between phases Q_{21} is negligible. Therefore, it may be stated that the considered discharging process is slow and that the non-equilibrium effects play no significant role. Consequently, the discrepancy between the pressure curves computed by the equilibrium model and the non-equilibrium model is small as presented in Fig. 14d. The computed results for pressure p in the steam accumulator are compared with corresponding measured data in Fig. 14b. As presented, good agreement is obtained. Further, it can be seen that computational results for pressure p overlap for cases $a_{in} = a_{in,orig}$ and $a_{in} = a_{in,mod}$.

Here is summarized that according to the results presented in Figs. 8c, 10c and 13c the application of the correction factor for the interfacial area concentration χ changes the evaporation and condensation relaxation factors in a wide range, from about 1 s (Fig. 13c), to the values of about 10 s (Fig. 8c) and 85 s (Fig. 10c), in the whole range of experimentally evaluated values presented in Table 5.

4.2. Analysis of closure law for evaluation of heat transfer rate due to temperature difference between phases

This Section deals with the evaluation of single-phase heat transfer rate due to temperature difference between liquid water and steam Q_{21} formulated by Eq. (31). The term to be assessed in this closure assumption is the product of heat transfer coefficient and interfacial area concentration $(ha)_{21}$. As presented in Section 2.1.2.2 there are two approaches for evaluation of this term: (i) the constant value of the product $(ha)_{21} = 50 \cdot 10^3 \text{ W/m}^3\text{K}$ is adopted or (ii) the values of heat transfer coefficient h_{21} and interfacial area concentration a_{21} are separately evaluated.

In this Section, the validity of these approaches is tested for charging of steam accumulator reported as Case B by Sun et al. [4] (see Table 8). Based on the results from the previous Section, the interfacial area concentration is evaluated using its modified formulation, $a_{21} = a_{in,mod}$ given by Eq. (46). The obtained results, presented in Fig. 15a–b, show that the values of Q_{21} computed by either of the two approaches are similar and that the resulting pressure curves overlap showing good agreement with measured values. Based on these considerations it may

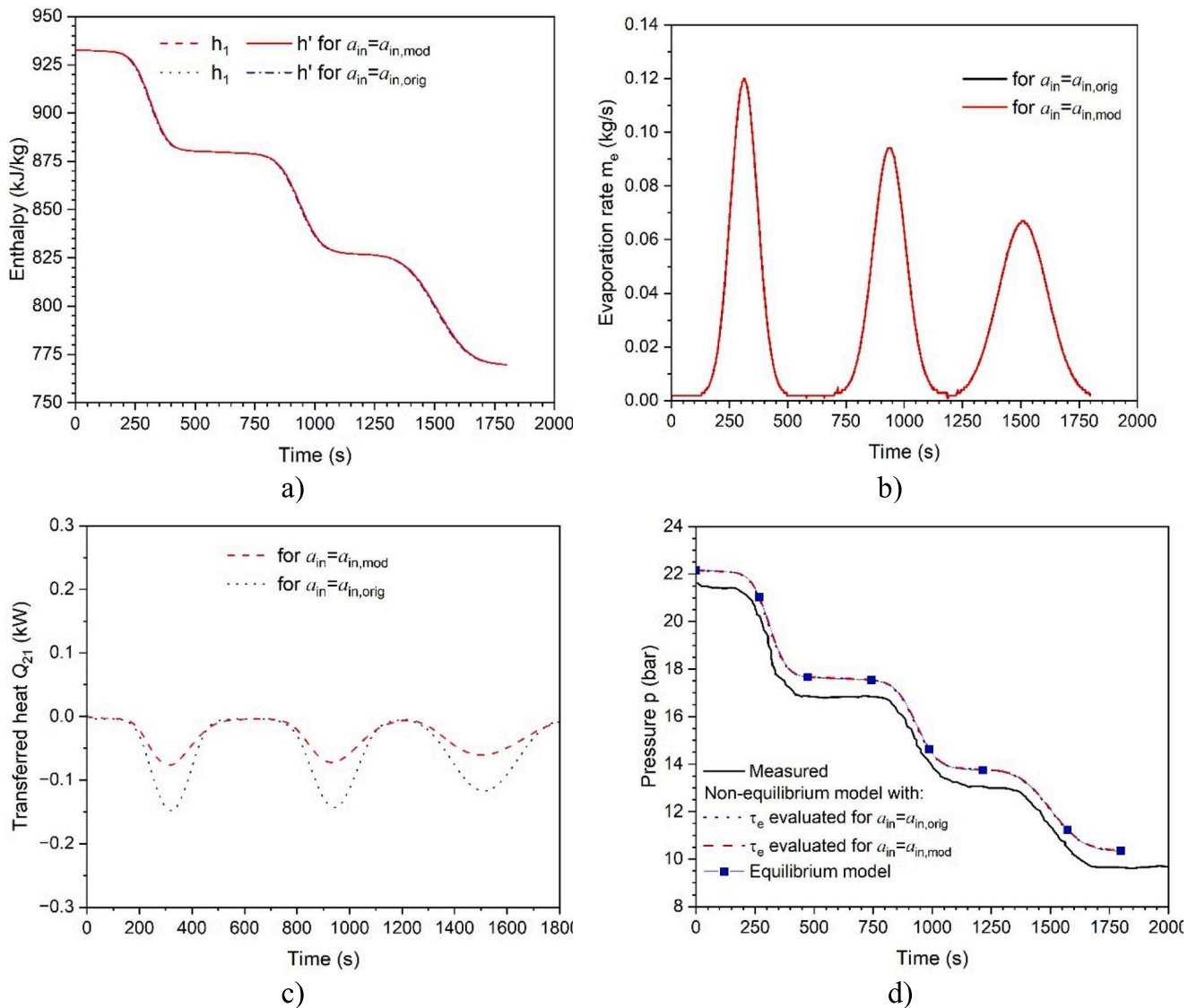


Fig. 14. Effect of modifying interfacial area on the evolution of main quantities during discharging of steam accumulator with small volume. The comparison of computed and measured pressure evolution is presented in graph d. Discharging conditions and geometrical data are adopted from [14] (see Table 7).

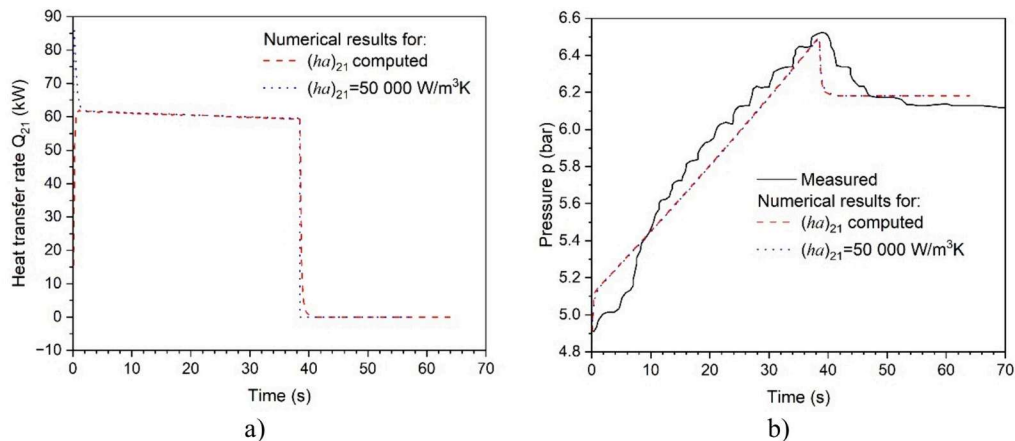


Fig. 15. Heat transfer rate due to temperature difference between phases (a) and pressure evolution (b) evaluated for conditions of steam accumulator charging reported as Case B in [4] (see Table 8).

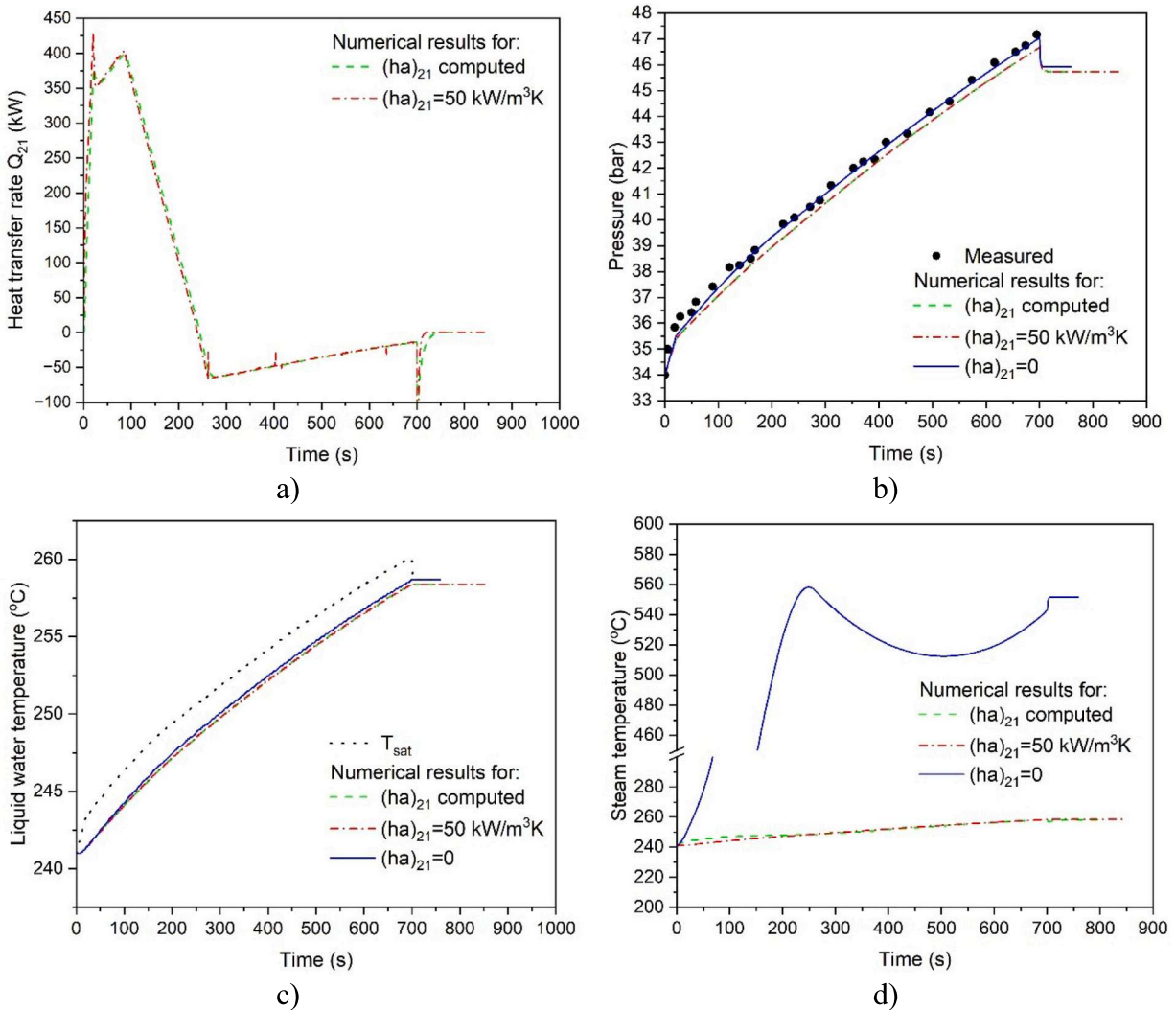


Fig. 16. Effect of accounting for heat transfer rate due to temperature difference between phases Q_{21} on main steam accumulator quantities. Charging conditions and steam accumulator geometry are adopted from [2] (see Fig. 4 and Table 6).

be stated that relation (32) for $(ha)_{21}$ proposed by Stevanovic et al. [3] performs well.

Regarding the term Q_{21} itself, we would like to emphasize that it may not be neglected in the energy balance equations, especially when the steam accumulator is charged with steam of high superheat. Here the importance of accounting for Q_{21} is pointed out using the case of charging large steam accumulator presented by Stevanovic et al. [2] as example (see Table 6 and Fig. 4). For that purpose, three scenarios are considered in which Q_{21} is evaluated: (i) using values of $(ha)_{21}$ as computed by Eq. (32), (ii) adopting the constant value $(ha)_{21} = 50 \cdot 10^3 \text{ W/m}^3\text{K}$ and (iii) using zero value of $(ha)_{21}$. The obtained results presented in Fig. 16 show that Q_{21} takes high values at the beginning of the transient, but then strongly falls down. However, as presented in Fig. 16b and c, accounting for or neglecting Q_{21} practically has no effect on the pressure p and the liquid water temperature T_1 . On the other side, the temperature of steam T_2 increases strongly to unrealistically high values when Q_{21} is neglected as can be seen in Fig. 16d (note that these values of T_2 are significantly higher than the temperature of charging steam $T_{2,in}$).

In order to explain this unphysical situation, we rely on the so-called equilibrium mass transfer rate per unit volume [19] given by:

$$\Gamma_{eE} = \frac{\rho}{r} \left[\frac{1}{\rho} - x \left(\frac{dh_2}{dp} \right)_{\text{sat}} - (1-x) \left(\frac{dh_1}{dp} \right)_{\text{sat}} \right] \frac{dp}{dt}, \quad (47)$$

where subscript E indicates that Γ_{eE} is derived for two-phase mixture in thermal equilibrium, while the subscript sat denotes saturation conditions. We note that Γ_{eE} represents the maximum possible evaporation rate per unit volume. Therefore, assuming that $\Gamma_{cE} = -\Gamma_{eE}$, the maximum condensation rate can be determined as:

$$m_{cE} = \Gamma_{cE} V. \quad (48)$$

The comparison of m_{cE} evaluated from Eq. (48) and m_c computed by the non-equilibrium model I in which Q_{21} is neglected shows good agreement as presented in Fig. 17. This means that condensation rate m_c , as the only way of heat exchange between phases in this case, achieved its maximal rate m_{cE} . As Q_{21} is neglected, the surplus energy brought by charging steam inflow $(mh)_{2,in}$ is used to increase steam enthalpy h_2 , which results in artificially high values of steam temperature T_2 as seen in Fig. 16d. This steam enthalpy increase does not lead to significant pressure increase because the mass of liquid phase M_1 is much larger than the one of steam M_2 (for instance, in initial state $t = 0 \text{ s}$, $M_{10} = 44,690.9 \text{ kg}$ and $M_{20} = 152.7 \text{ kg}$).

5. Conclusions

The analyses of numerical models for the computation of steam accumulator dynamics presented in this paper have pointed out to two

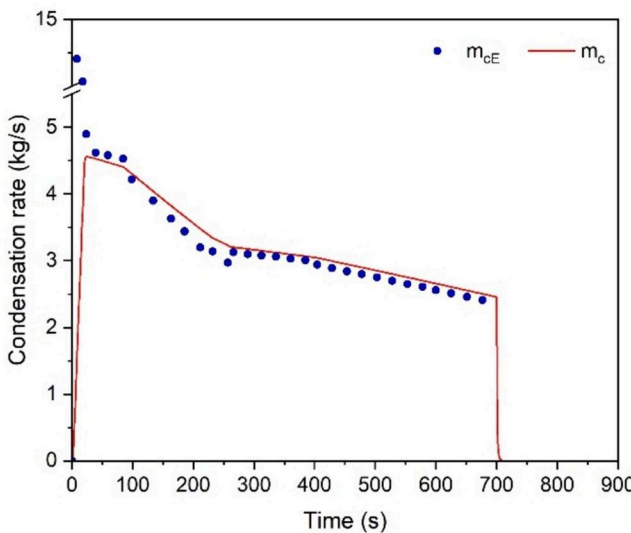


Fig. 17. Condensation rate for conditions of zero heat transfer rate Q_{2i} : m_c computed by non-equilibrium model I, m_{cE} evaluated by relation (48). Charging conditions and steam accumulator geometry are adopted from [2] (see Fig. 4 and Table 6).

critical issues. The first one is related to the models themselves. Therefore, the equilibrium model is appropriate only for slow transients in which non-equilibrium effects are not pronounced. In that sense, the use of the non-equilibrium models is recommended. However, when applying this modelling approach, caution is necessary as here performed analyses have shown that: (i) the governing equation for energy needs to be formulated properly with all balance terms included and (ii) closure laws for the phase transition rate are of limited applicability. Regarding the latter, in this paper an improved formulation of closure assumption for the condensation rate during charging transient is proposed and validated by available data obtained by measurements on steam accumulators of small and large size.

The second critical issue is associated with the serious lack of experimental data on steam accumulator dynamics. Regarding that, we emphasise that the conduction of such investigations in the future are of great importance. Further, we would like to point out that the construction of specific test sections for experimental investigations of the steam accumulator dynamics should be neither the only nor the preferred way for the following reasons. As steam accumulator vessels in experimental test sections are commonly of small size, the applicability of measured data would be limited because the dynamics of steam

accumulators depends much on its volume as shown in this paper. In relation to that, we propose the conduction of experimental runs also on large steam accumulators, which have already been installed and are in operation in number of industrial facilities. Having measured data on both, lab-type and industrial, steam accumulators would provide the valuable basis for further validation of existing and development of improvement modelling approaches.

Future research should be based on a wide experimental campaign with measurements at various charging/discharging transients with the goal to provide deeper insights into thermal-hydraulic mechanisms influenced by the interplay of geometrical characteristics and operating conditions of the steam accumulators. This will lead to improved interfacial closure laws which account for currently not included effects such as: the effect of the steam injection system design on the condensation rate, the effect of thickness of the pressure vessel walls on heat transfer from the liquid water/steam especially in the vicinity of the water mirror, the effect of aspect ratio (ratio of steam accumulator diameter and length) i.e. the height of the liquid column and the size of the free surface on the condensation/evaporation process, etc. The pressure level also plays an important role as it affects water physical quantities (for example, at higher pressure the latent heat of evaporation/condensation decreases).

CREDIT authorship contribution statement

Milica Ilic: Writing – original draft, Methodology, Investigation, Conceptualization. **Vladimir D. Stevanovic:** Methodology, Investigation, Conceptualization. **Milan M. Petrovic:** Visualization, Software, Resources. **Sanja Milivojevic:** Visualization, Software, Resources.

Declaration of competing interest

The authors declare that they have no known competing financial interests or personal relationships that could have appeared to influence the work reported in this paper.

Data availability

Data will be made available on request.

Acknowledgments

This research was supported by the Science Fund of the Republic of Serbia, #GRANT No 3434, Improving operational flexibility of decarbonized thermal power plants with energy storage toward increased renewable sources utilization – TPP-RSU.

Appendix 1

An open thermodynamic system is schematically presented in Fig. A1 as the control volume CV with the deformable boundary cv , with inlets $i = 1, N$ and outlets $j = 1, K$. The general form of the first law of thermodynamics for this system is given by [20]:

$$\frac{dE_{CV}}{dt} = Q - W + \sum_i m_{in,i} \left(u_{in,i} + \frac{w_{in,i}^2}{2} + gz_{in,i} \right) - \sum_j m_{out,j} \left(u_{out,j} + \frac{w_{out,j}^2}{2} + gz_{out,j} \right). \quad (\text{A1})$$

Eq. (A1) represents energy conservation law which states that the time rate of change of total energy contained within the control volume dE_{CV}/dt is equal to the sum of rates at which energy is being transferred by the heat transfer Q , by the work W and by the mass flow streams entering the control volume (third term on the r.h.s. of Eq. A1) and exiting the control volume (fourth term on the r.h.s. of Eq. A1). In Eq. (A1) the following notation applies: m represents the mass flow rate, u stands for the specific internal energy, w is the velocity, while g and z respectively represent the gravity and the vertical coordinate. The subscripts in,i and out,j denote i -th inlet and j -th outlet. It is noted that the subscript CV indicates the control volume and should not be confused with the subscript cv which is used to denote the deformable control volume boundary in Fig. A1 and text below.

The total energy contained within the control volume is given by $E_{CV} = (\rho Ve)_{CV}$, where ρ denotes the density, V stands for the volume, while the total energy per unit mass e_{CV}

$$e_{CV} = u_{CV} + \frac{w_{CV}^2}{2} + gz_{CV}, \quad (A2)$$

represents the sum of internal energy u , kinetic energy $ke = w^2/2$ and potential energy $pe = gz$.

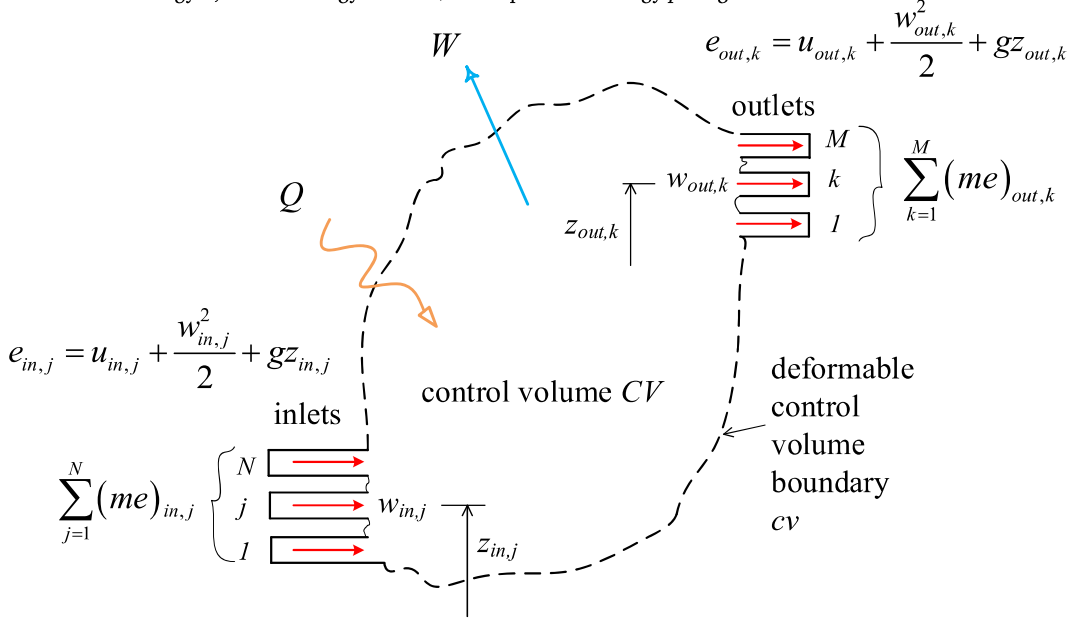


Fig. A1. Schematic presentation of an open thermodynamic system.

The terms Q and W in Eq. (A1) represent net energy rates over the boundary of control volume for which the following convention applies: Q is negative if it is transferred from the system and W is negative if it is done by surrounding to the system. While Q accounts for the heat transfer rate across the whole cv boundary ($Q = Q_{cv}$), the term W is decomposed as:

$$W = \sum_j m_{out,j} \left(\frac{p}{\rho} \right)_{out,j} - \sum_i m_{in,i} \left(\frac{p}{\rho} \right)_{in,i} + W_{cv}, \quad (A3)$$

where the first two terms on the r.h.s. of Eq. (A3) represent the energy transfer due to the work at inflow and outflow boundaries (the derivation of these terms is given elsewhere, see for example [20,21]), while the term W_{cv} stands for the contribution across the rest of control volume boundary. The term W_{cv} encompasses various forms of the work as given below by Eq. (A4): the work transferred to the control volume through displacement of its boundaries by pressure forces, W_{press} , by a rotating shaft, W_{shaft} , or by viscous forces, W_{visc} . The last term, W_{other} , involves the energy transfer by work of other forces such as the electric force, the magnetic force, the surface tension, etc.

$$W_{cv} = W_{press} + W_{shaft} + W_{visc} + W_{other}. \quad (A4)$$

For conditions of the steam accumulator, the following may be assumed.

- Only W_{press} is of importance, while all other terms in Eq. (A4) are negligible. Therefore,

$$W_{cv} = W_{press} = \left(p \frac{dV}{dt} \right)_{cv}. \quad (A5)$$

- Kinetic and potential energy may be neglected for the control volume as well as for its inflow and outflow boundaries. Therefore,

$$\frac{w_k^2}{2} + gz_k = 0 \text{ for } k = CV \text{ or in, i or out, j.} \quad (A6)$$

Applying the above assumptions Eq. (A1) is transformed to:

$$\frac{d(Mu)_{cv}}{dt} = Q_{cv} - \left(p \frac{dV}{dt} \right)_{cv} + \sum_i m_{in,i} \left(u + \frac{p}{\rho} \right)_{in,i} - \sum_j m_{out,j} \left(u + \frac{p}{\rho} \right)_{out,j}, \quad (A7)$$

where $M_{CV} = (\rho V)_{CV}$ represents the mass of control volume. Inserting the enthalpy $h = u + p/\rho$ Eq. (A7) can be rearranged to:

$$\frac{d(Mh)_{cv}}{dt} = Q_{cv} + \left(V \frac{dp}{dt} \right)_{cv} + \sum_i m_{in,i} h_{in,i} - \sum_j m_{out,j} h_{out,j}. \quad (A8)$$

References

- [1] W.-D. Steinmann, Thermal Energy Storage for Medium and High Temperatures - Concepts and Applications, Springer, 2022, <https://doi.org/10.1007/978-3-658-02004-0>.
- [2] V.D. Stevanovic, B. Maslovaric, S. Prica, Dynamics of steam accumulation, *Appl. Therm. Eng.* 37 (2012) 73–79, <https://doi.org/10.1016/j.applthermaleng.2012.01.007>.
- [3] V.D. Stevanovic, M.M. Petrovic, S. Milivojevic, B. Maslovaric, Prediction and control of steam accumulation, *Heat Transf. Eng.* 36 (2015) 498–510, <https://doi.org/10.1016/j.enconman.2020.113271>.
- [4] B. Sun, J. Guo, Y. Lei, L. Yang, Y. Li, G. Zhang, Simulation and verification of a non-equilibrium thermodynamic model for a steam catapult's steam accumulator, *Int. J. Heat Mass Transf.* 85 (2015) 88–97, <https://doi.org/10.1016/j.ijheatmasstransfer.2015.01.120>.
- [5] V.S.P. Raphael, R. Velraj, P. Jalihal, Transient analysis of steam accumulator integrated with solar based MED-TVC system, *Desalination* 435 (2018) 3–22, <https://doi.org/10.1016/j.desal.2017.12.045>.
- [6] M. Richter, G. Oeljeklaus, K. Görner, Improving the load flexibility of coal-fired power plants by the integration of a thermal energy storage, *Appl. Energy* 236 (2019) 607–621, <https://doi.org/10.1016/j.apenergy.2018.11.099>.
- [7] V.D. Stevanovic, M.M. Petrovic, S. Milivojevic, M. Ilic, Upgrade of the thermal power plant flexibility by the steam accumulator, *Energy Convers. Manag.* 223 (2020) 113271, <https://doi.org/10.1016/j.enconman.2020.113271>.
- [8] Q. Yu, X. Li, Z. Wang, Q. Zhang, Modeling and dynamic simulation of thermal energy storage system for concentrating solar power plant, *Energy* 198 (2020) 117183, <https://doi.org/10.1016/j.energy.2020.117183>.
- [9] E. Xu, Z. Wang, G. Wei, J. Zhuang, Dynamic simulation of thermal energy storage system of Badaling 1 MW solar power tower plant, *Renew. Energy* 39 (2012) 455–462, <https://doi.org/10.1016/j.renene.2011.08.043>.
- [10] M. Stark, F. Conti, A. Saidi, W. Zörner, R. Greenough, Steam storage systems for flexible biomass CHP plants - evaluation and initial model based calculation, *Biomass Bioenergy* 128 (2019) 105321, <https://doi.org/10.1016/j.biombioe.2019.105321>.
- [11] P.A. Gonzalez-Gomez, M. Laporte-Azcue, M. Fernandez-Torrijos, D. Santana, Hybrid storage solution steam-accumulator combined to concrete-block to save energy during startups of combined cycles, *Energy Convers. Manag.* 253 (2022) 115168, <https://doi.org/10.1016/j.enconman.2021.115168>.
- [12] A.A. Kindi, P. Sapin, A.M. Pantaleo, K. Wang, C.N. Markides, Thermo-economic analysis of steam accumulation and solid thermal energy storage in direct steam generation concentrated solar power plants, *Energy Convers. Manag.* 274 (2022) 116222, <https://doi.org/10.1016/j.enconman.2022.116222>.
- [13] S. Dusek, R. Hofmann, Modeling of a hybrid steam storage and salidation with an industrial Ruths steam storage line, *Energies* 12 (2019) 1014, <https://doi.org/10.3390/en12061014>.
- [14] L. Kasper, D. Pernsteiner, A. Schirrer, S. Jakubek, R. Hofmann, Experimental characterization, parameter identification and numerical sensitivity analysis of a novel hybrid sensible/latent thermal energy storage prototype for industrial retrofit applications, *Appl. Energy* 344 (2023) 121300, <https://doi.org/10.1016/j.apenergy.2023.121300>.
- [15] P.H. Niknam, A. Sciacovelli, Hybrid PCM-steam thermal energy storage for industrial processes – link between thermal phenomena and techno-economic performance through dynamic modelling, *Appl. Energy* 331 (2023) 120358, <https://doi.org/10.1016/j.apenergy.2022.120358>.
- [16] Yu.N. Kuznecov, *Heat Transfer in Safety Problems of Nuclear Reactors*, Energoatomizdat, Moscow, 1989 (in Russian).
- [17] N. Zuber, J.A. Findlay, Average volumetric concentration in two-phase flow systems, *J. Heat Transf.* 87 (1965) 453–468, <https://doi.org/10.1115/1.3689137>.
- [18] V.N. Blinkov, S.D. Frolov, Modeling of flashing flow in nozzles, *Eng. Phys. J.* 42 (1982) 741–746 (in Russian).
- [19] P. Berne, Critical analysis of evaporation rate applied in computations of two-phase flows in conduit, in: Report CEA-R-5205, CEN, Grenoble, France, 1983 (in French).
- [20] M.J. Morgan, H.N. Shapiro, D.D. Boettner, M.B. Bailey, *Fundamentals of Engineering Thermodynamics*, Seventh edition, John Wiley & Sons Inc., 2011.
- [21] Y.A. Cengel, M.A. Boles, M. Kanoglou, *Thermodynamics - An Engineering Approach*, Ninth edition, McGraw Hill Education, 2019.
- [22] A.R. Edwards, *Conduction Controlled Flashing of a Fluid and the Prediction of Critical Flow Rates in a One-Dimensional System*, UKAEA, Health & Safety Branch, 1968, p. R147.
- [23] M.M. Petrovic, V. Stevanovic, Coupled two-fluid flow and wall heat conduction modeling of nucleate pool boiling, *Numer. Heat Transf. A* 80 (2021) 63–91, <https://doi.org/10.1080/10407782.2021.1935047>.
- [24] K. Wolfert, The simulation of blowdown processes with consideration of thermodynamic nonequilibrium phenomena, *Proc. of the CSNI Specialists Meeting, Atomic Energy of Canada 1* (1976) 156–194.
- [25] S. Banerjee, A surface renewal model for interfacial heat and mass transfer in transient two-phase flow, *Int. J. Multiphase Flow* 4 (1978) 571–573, [https://doi.org/10.1016/0301-9322\(78\)90016-2](https://doi.org/10.1016/0301-9322(78)90016-2).
- [26] S.M. Ghiaasiaan, *Two-Phase Flow, Boiling and Condensation*, Cambridge University Press, 2008, pp. 52–55.